# Decadal Analysis Produced from an Ocean Data Assimilation System

A. ROSATI, R. GUDGEL, AND K. MIYAKODA

*GFDL/NOAA, Princeton University, Princeton, New Jersey*

## ABSTRACT

A global oceanic four-dimensional data assimilation system has been developed for use in initializing coupled ocean–atmosphere general circulation models and also to study interannual variability. The data inserted into a high-resolution global ocean model consist of conventional sea surface temperature observations and vertical temperature profiles. The data are inserted continuously into the model by updating the model's temperature solution every time step. This update is created using a statistical interpolation routine applied to all data in a 30-day window for three consecutive time steps and then the correction is held constant for nine time steps. Not updating every time step allows for a more computationally efficient system without affecting the quality of the analysis.

The data assimilation system was run over a 10-yr period from 1979 to 1988. The resulting analysis product was compared with independent analysis including model-derived fields like velocity. The large-scale features seem consistent with other products based on observations. Using the mean of the 10-yr period as a climatology, the data assimilation system was compared with the Levitus climatological atlas. Looking at the sea surface temperature and the seasonal cycle, as represented by the mixed-layer depth, the agreement is quite good, however, some systematic differences do emerge.

Special attention is given to the tropical Pacific examining the El Niño signature. Two other assimilation schemes based on the coupled model using Newtonian nudging of SST and then SST and surface winds are compared to the full data assimilation system. The heat content variability in the data assimilation seemed faithful to the observations. Overall, the results are encouraging, demonstrating that the data assimilation system seems to be able to capture many of the large-scale general circulation features that are observed, both in a climatological sense and in the temporal variability.

## 1. Introduction

As the availability of ocean data increases dramatically in quality and quantity in the near future, and both ocean and atmosphere models improve, the predictability of the coupled ocean–atmosphere system becomes feasible. The long-term goal of our work is to provide a description, understanding, and prediction of the coupled system as complete and reliable as that which now exists for the atmosphere alone. In weather forecasts, it has been customary to use data assimilation methods for generating initial conditions. For forecasts with coupled air–sea general circulation models (GCM), it would also be reasonable to consider that the ocean and atmosphere data assimilation (DA) are the optimum methods for the production of initial conditions even though the variability of the coupled system is quite different from any simple function of its parts (Ghil et al. 1991). As the first step toward this

goal, a scheme of the oceanographic DA was developed by Derber and Rosati (1989).

This paper is a report on the implementation of this technique to a long-time series of ocean data analysis. The period of the analysis is 10 years from January 1979 to December 1988. During the decade, various national and international projects of data acquisition and processing were carried out—that is, COADS, MOODS, TOGA, and FOCAL. (The acronyms and the contents will be described later.) These datasets are utilized for this study. We will examine the utility of the DA system both as a climatology and for capturing temporal variation.

Another objective of this paper is to compare Derber and Rosati's variational method DA system with simpler methods—that is, the Newtonian nudging of the coupled system using (a) observed SSTs and (b) observed SSTs and surface winds. If either of the two nudging methods prove to be comparable to the DA in terms of the analysis quality, the technique of nudging can be a viable option for the generation of initial conditions and production of the climatic dataset of ocean analysis.

The assimilating model along with the surface forcing and oceanic data are described in section 2. This

*Corresponding author address:* Dr. Kikuro Miyakoda, Geophysical Fluid Dynamics Laboratory, Princeton University, Forrestal Campus, US Route 1, P.O. Box 308, Princeton, NJ 08542.
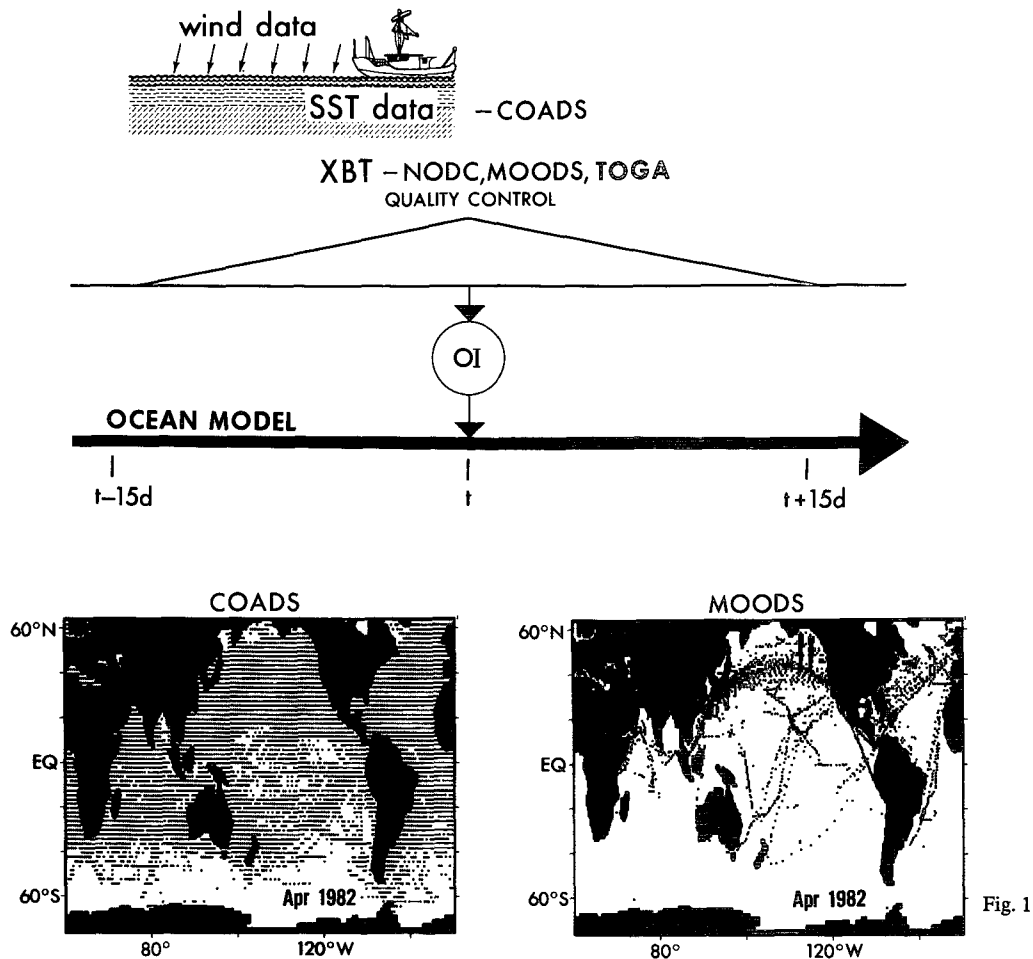E-mail: km@gfdl.gov

FIG. 1. Schematic illustration of Derber–Rosati data assimilation system. Various data—i.e., COADS, NODC, MOODS, and TOGA—are processed by quality control and are injected into the model using a 30-day window. The spatial interpolation between the observation locations and grid is performed by the optimum interpolation (OI) scheme. The lower portion shows examples of the surface temperature data (from COADS) and subsurface temperature profiles (from MOODS) for April 1982.

system is essentially the same as the one in Derber and Rosati (1989) with a modification to the frequency of inserting the temperature correction that results in a computational savings. As in the previous study, the ocean data has been limited to conventional surface temperature data and vertical temperature profiles. The following three sections (3, 4, 5) examine the results looking at a comparison to independent observed analysis, for instantaneous and decadal means, and finally the interannual variability in the tropical Pacific. For the tropical Pacific, the heat content from the coupled model SST nudging is compared to the DA system. The summary notes discuss the utility of the DA system.

## 2. Data assimilation systems

### a. DA system for an ocean model

The ocean model configuration is the same as described in Rosati and Miyakoda (1988). The model

equations were solved on a nearly global grid (excluding the Arctic Ocean) with realistic topography. In the horizontal, a staggered $1° \times 1°$ latitude–longitude grid was used except between $10°N$ and $10°S$ where the north–south resolution was increased to $1/3°$ in order to resolve finer-scale equatorial structures. The model includes subgrid-scale parameterizations, nonlinear viscosity for horizontal mixing, and turbulence closure scheme for vertical mixing.

The atmospheric forcing consists of the surface wind stress and surface heat flux. The surface wind, temperature, and moisture data were obtained from the twice-daily analysis of the National Meteorological Center (NMC). The method for computing heat flux is described in detail in Rosati and Miyakoda. Note that the quality of NMC data during this 10-yr period was not very good although it improved during the latter years. Also, since the NMC analysis scheme changed over
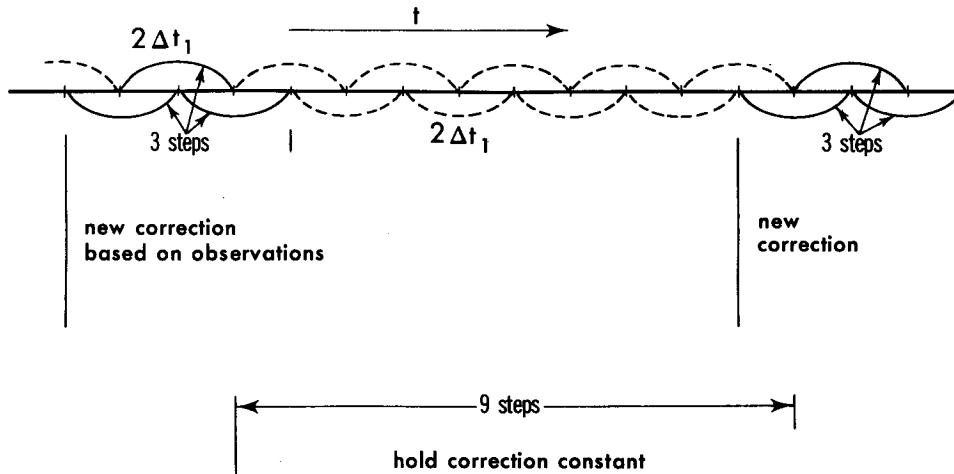
FIG. 2. Illustration of the economical assimilation method. The correction due to the observation is calculated only for the first three time steps, and the same value at the third step is used repeatedly in the subsequent nine time steps.

this period many times, the resultant dataset is not self-consistent.

In this study, the oceanic data have been limited to conventional surface temperature data and vertical temperature profiles. The ocean surface temperature data for the entire 10 years are taken from COADS (Comprehensive Ocean–Atmosphere Data Set, see Woodruff et al. 1987). An example is shown in Fig. 1; the dots represent the sea surface data of COADS. The SST data were monthly averaged data within $2° \times 2°$ latitude–longitude quadrangles. As can be seen, the data coverage is very sparse over the Southern Ocean; therefore, the analysis in this region would tend to be less accurate. This situation could be alleviated by the inclusion of satellite data; however, blending of this field would require the understanding of the satellite errors—that is, day versus night bias and attenuation correction (Reynolds et al. 1989). Such an investigation is beyond the scope of this paper.

The vertical temperature profiles are based on the subsurface water temperatures measured mainly by merchant, fishing, and research vessels (see White et al. 1985; Kessler 1989), and here, taken from three sources of dataset. They are NODC (the National Oceanic Data Center) for 5 years from 1984 to 1988, U.S. Navy's MOODS (Master Oceanic Observation Data Set, see Bauer 1985) for 6 years from 1979 to 1984, and TOGA (Tropical Ocean and Global Atmosphere Project) dataset for 4 years from 1985 to 1988. The subsurface data can be identified by the dark ship tracks of the MOODS dataset shown in Fig. 1. This is a typical example of the monthly coverage from the three datasets. The XBT (expendable bathythermograph) profiles normally extend to about a depth of 450 m.

The observed data were continuously inserted into the ocean model by applying a correction to the forecast temperature field at every model time step. The spatial objective analysis technique is based on the statistical interpolation analysis scheme of Gandin (1966). The method used by Derber and Rosati is based on the variational principle (Sasaki 1958; Lorenc 1986), in which the ocean model solutions are used as the first guess for temperature and the final analysis is determined by the inserted oceanographic data in such a way that a functional is statistically minimal. The functional consists of two terms: first, the fit of the corrected temperature field to the guess field weighted by an estimate of the first guess error covariance matrix, and second, the fit of the corrected temperature field to the observations weighted by the observational error covariance matrix. The functional is minimized using a conjugate gradient algorithm. Error estimates, which determine the spatial structure and amplitude of the correction field, are specified for each observation and for the first guess. The observational error covariances are set equal to an estimate of the observational error variance. This variance estimate is taken from the COADS estimate for the SSTs. For the temperature profiles, the variance is set equal to $(0.25°C)^2$. These error estimates are then weighted by a time factor that increases linearly from 0 to 1 and back to 0 as the difference between the observation time and the model solution time goes from $-15$ days to 0 to $+15$ days. The observations are given no weight when the time difference is greater than 15 days. The inclusion of the time factor allows the use of 30 days of observations in the analysis scheme, yet gives the observations closest to the present model time step more weight. This has the built-in assumption that ones interest is in the low-frequency phenomena. Currently, the first-guess error covariance matrix is defined so that the vertical correlations are ignored and the spatial correlations are assumed to be the same for each
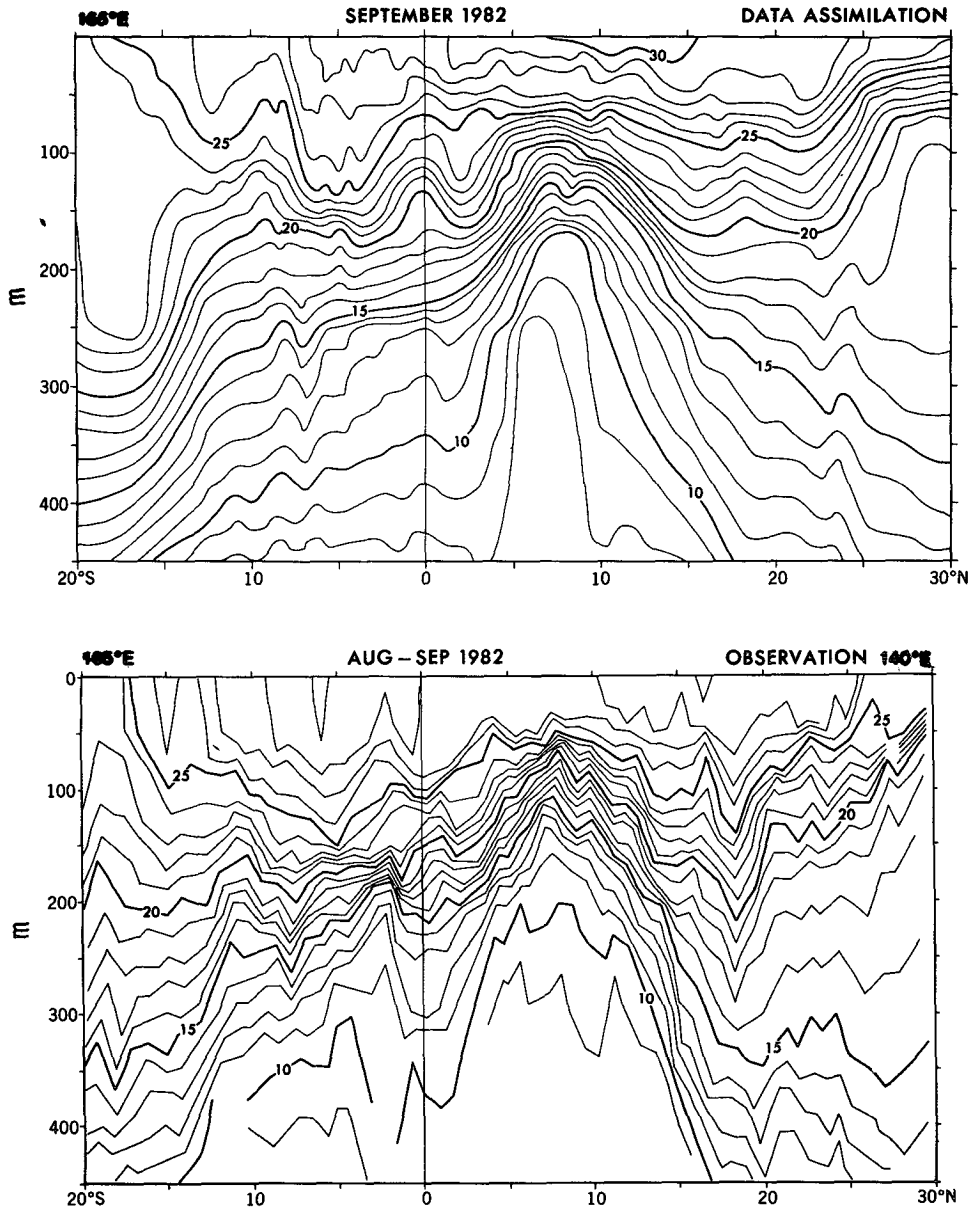
FIG. 3. Temperature distributions at depth near 155°E for September 1982: (upper) data assimilation; (lower) direct plot of temperature profile by ship measurement. Contour interval is 1°C.

model level. The horizontal covariances are defined by a Gaussian with an $e$-folding scale of 2° at the equator. This decreases away from the equator by the cosine of the latitude allowing for smaller-scale features in the corrections at higher latitudes. Unfortunately these statistics are not well known and, thus, are now defined empirically. As these statistics become better defined, the results should also improve.

In addition, the climatological salinity, taken from Levitus (1982), is specified at the surface through the boundary condition (at $z = 0$); that is,

$$\frac{\partial s}{\partial z} \propto s_{\text{clim}} - s, \tag{2.1}$$

where $s$ is the salinity and $s_{\text{clim}}$ is the climatological salinity. Of course, this is an ad hoc arrangement; it is hoped that in the future observed salinity data will be used. [Carton and Hackert (1990) included observed salinity data in their data assimilation.]

Assembling the observed data from within a 15-day interval to either side of the current time step, the ocean data are injected into the model (Fig. 1). The time step
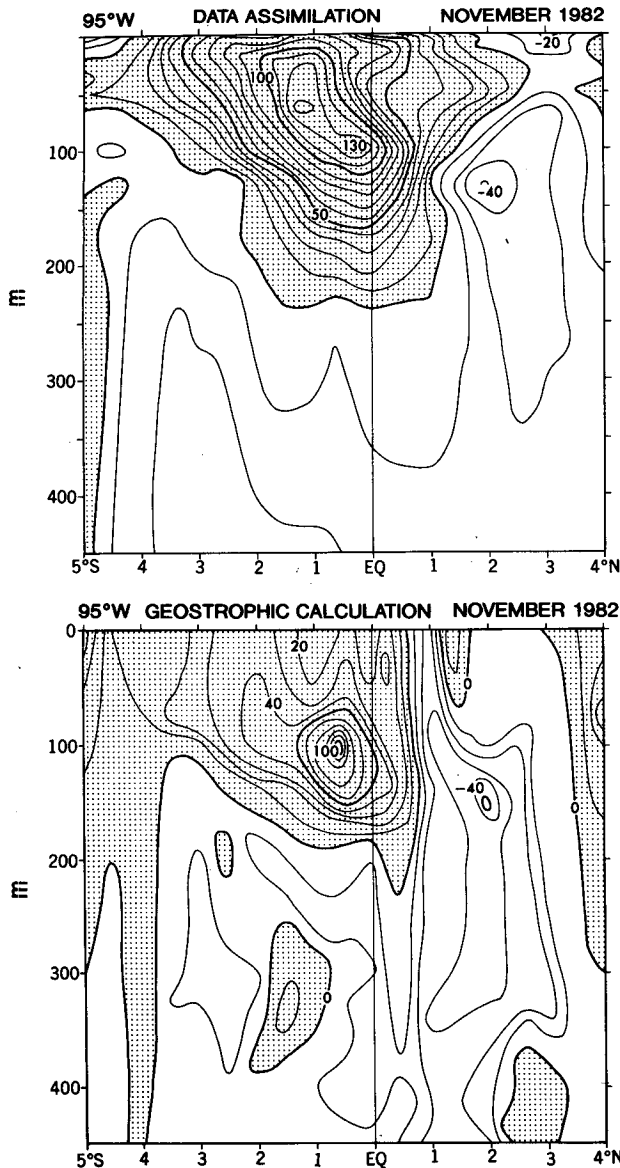
FIG. 4. Isotachs of zonal current at depth along 95°W for November 1982: (upper) data assimilation; (lower) the geostrophic calculation. Contour interval is 10 cm s$^{-1}$. Eastward currents are stippled.

for integrating the temperature and salinity equations is $\Delta t_1 = 2$ h, while the time step for the momentum equation is $\Delta t_2 = 1$ h. Thus, the model runs continuously, while the observation data are injected into the model.

Unfortunately the solving of the minimization of the functional by the conjugate gradient method is quite time consuming, although this technique itself is extremely efficient. To save computer time, the assimilation procedure is skipped for certain time steps. The temperature correction is computed for three consecutive time steps and then held constant for the subsequent nine time steps (see Fig. 2). Namely, the corrections to the first guess due to the

observed data are calculated in the first three steps—that is, 6 h ($=3\Delta t_1$)—and the correction values at the third step are saved. In the subsequent nine steps—that is, 18 h ($=9\Delta t_1$)—the saved values are used repeatedly as the correction to the model solutions. Tests revealed that this economized version gives practically the same solutions as when the corrections are computed every time step. With this process, all oceanographic variables such as the ocean currents, temperature, and salinity are determined consistently within the framework of the ocean GCM and the associated boundary conditions.

### b. Newtonian nudging

As an alternative to the full DA, a simple method—that is, Newtonian nudging—is investigated. In our case, the nudging technique is applied in two ways. One way is used for the coupled air–sea model, in which only the top level of the ocean model is nudged toward the observed SST. Specifically, the temperature equation for the upper-most layer of ocean model is modified by adding a Newtonian nudging term; that is,

$$\frac{\partial T}{\partial t} \cdots = -\lambda(T - T_{obs}),  \qquad (2.2)$$

where $\lambda$ is the Newtonian damping coefficient, (3 day)$^{-1}$, and $T_{obs}$ is the observed SST; $T_{obs}$ in this study is the monthly mean SST field of Reynolds (1982). This simplified DA is originally used for assessing the "systematic bias" of SST in the model. Integrating the model equations for 10 years with Eq. (2.2), the systematic bias or flux adjustment term is calculated based on the time averages of the term on the rhs of Eq. (2.2) (Miyakoda et al. 1989). Note that a similar approach was proposed by Sausen et al. (1988). The idea is that given a good SST field the surface winds generated from the atmospheric model would be close to reality and the subsurface ocean fields would be in balance with the model winds.

Another way of using the nudging technique is that not only SST data but also the surface wind stress data are used. Taking the same coupled air–sea model, two equations are modified. One is the Eq. (2.2). The other is the momentum equation in the lowest layer of the atmospheric GCM; that is,

$$\frac{\partial V}{\partial t} \cdots = -\mu(V - V_{obs}),  \qquad (2.3)$$

where $V$ is the wind vector; the term $-\mu(V - V_{obs})$ is the Newtonian nudging term; $\mu$ is the damping coefficient, $(1\ h)^{-1}$; and $V_{obs}$ is the observed wind vector. In this study, the NMC analysis of 12-h wind data at 1000-hPa level are utilized (as described above), and the nudging terms are applied only over the ocean surface, excluding land. In this approach, since the damping coefficients are chosen to strongly constrain the ocean
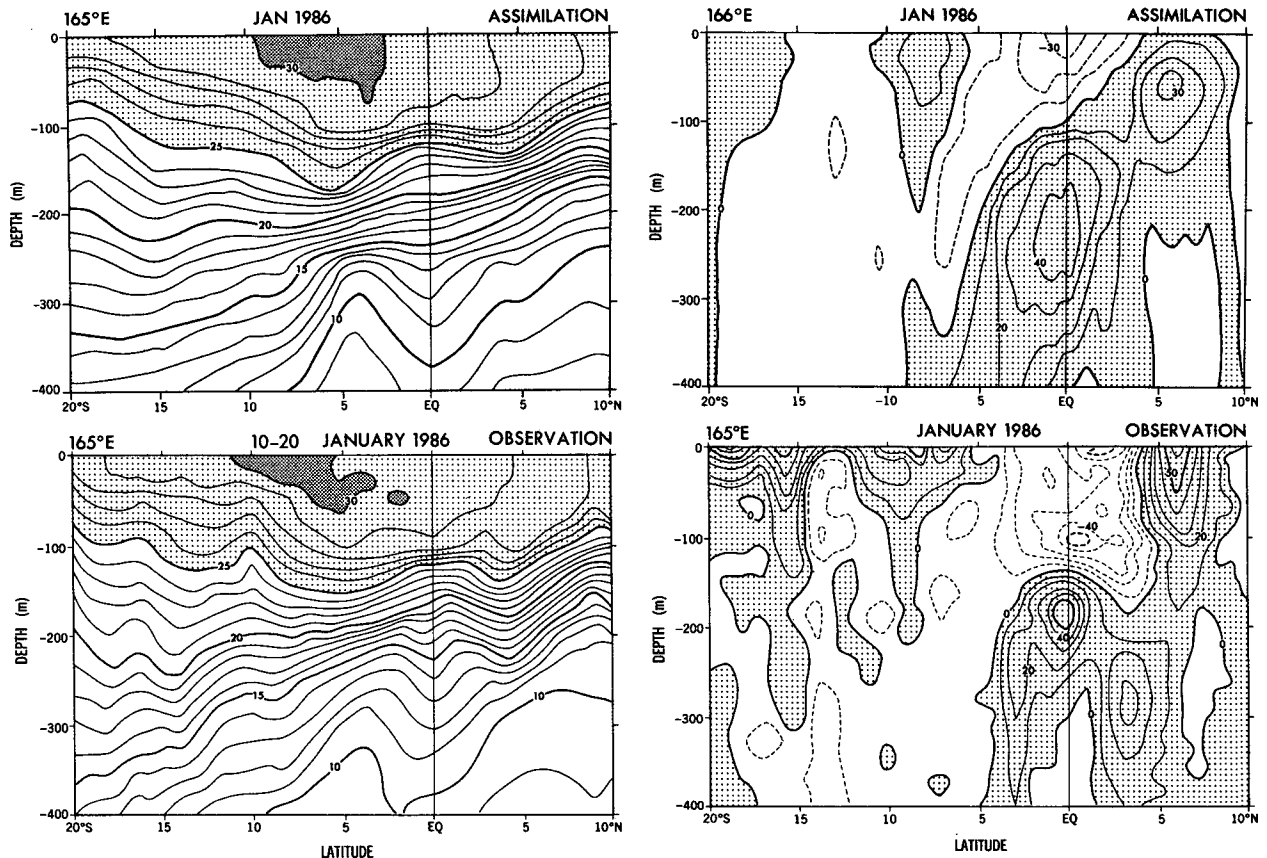
FIG. 5. (a) Isotherms along 165°E for January 1986: (upper) data assimilation; (lower) direct plots of temperature profile by ship measurement for 10–20 January (Delcroix et al. 1987). Contour interval is 1°C. (b) Isotachs of zonal current along 165°–166°E for January 1986: (upper) data assimilation; (lower) the direct observation (Delcroix et al. 1987). Contour interval is 10 cm s$^{-1}$. Eastward currents are stippled.

model's surface boundary conditions toward observations, the coupled air–sea model has little feedback and probably is not needed except for the insolation reaching the ocean surface. But for the purpose of comparison with the temperature nudging case, the same coupled model is employed for the SST–wind nudging case. The atmospheric spectral GCM, after Gordon and Stern (1982), is the T30L18.

The essential differences between the two nudging cases is that in the first case the ocean model is forced by the T30 atmospheric model winds that are consistent with observed SSTs and in the second case the ocean model is forced by NMC wind analysis.

### c. Execution of assimilations

The main objective is to produce an ocean analysis using DA for a given 10-yr period. In parallel, auxiliary runs are made with the *temperature nudging,* and also the *temperature-wind nudging,* for about the same 10 years. To execute these runs, initial conditions are required at $t = 0$—that is, 0000 UTC 1 January 1979. These conditions were generated by running the ocean

GCM for more than 9 years in the climatological mode, using climatological forcing—that is, the wind stress of Hellerman and Rosenstein (1983)—and nudging toward Levitus climatological SSTs. Nine years was sufficiently long for spinning up the ocean GCM, to attain quasi-equilibrium conditions for the upper ocean from the surface down to about 400-m depth.

For the temperature nudging and the temperature–wind nudging, additional initial conditions are required for the atmospheric model. These conditions are taken from the level III NMC analysis.

Some examples of the preliminary analysis based on this DA system were shown by Derber and Rosati (1989); however, this sequel paper examines the full decadal series of analysis, comparing to independent analyses. The results of the auxiliary runs will be shown by way of comparison.

### 3. Samples of the analysis

#### a. Meridional cross sections in the tropical Pacific

Figure 3 displays latitude–depth sections of temperature at about 155°E for September 1982. The lower
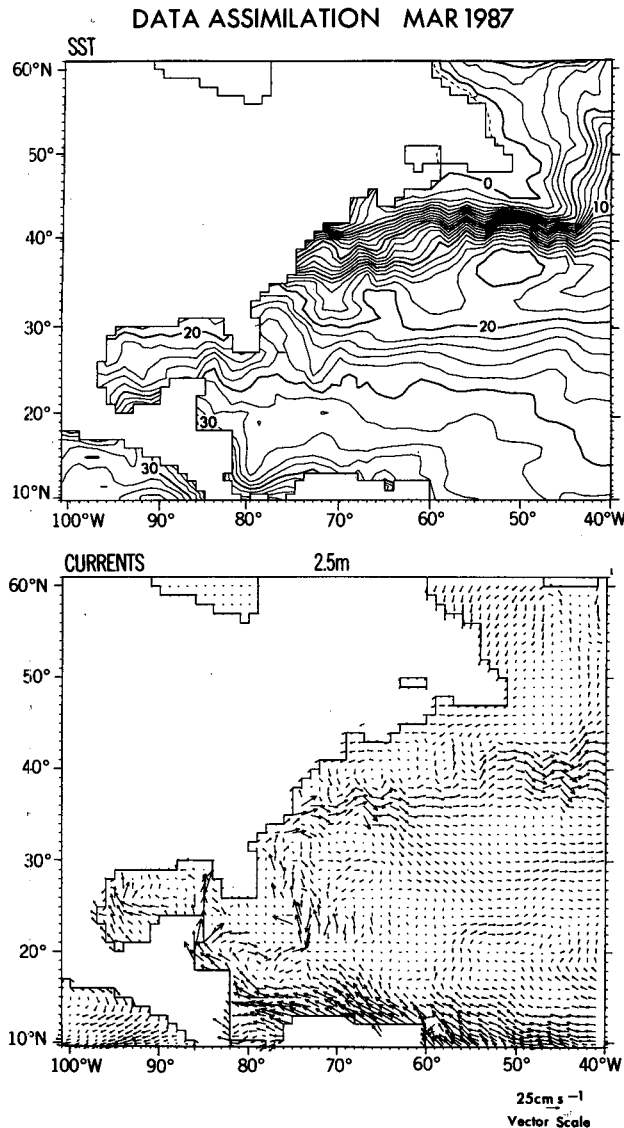
## DATA ASSIMILATION  MAR 1987



FIG. 6. An example of the DA analysis for March 1979: (upper) the isotherms; (lower) current vectors.

panel is a plot of connected observed vertical temperature profiles measured by a commercial ship, crossing at 30°N, 140°E (Japan) to 21°S, 166°E (New Caledonia) and taking 10 days or so in August and September. The upper panel is the monthly mean of the DA results along 155°E for September. It should be noted that this particular ship measurement was not included in the DA. The overall agreement between them is good, although within the upper 50 m the DA appears warmer, and the isothermal layers at 30°N and 18°S in the DA do not exist in the ship track; the reason for this discrepancy may be due to the winter convective overturning and will be discussed later.

Figure 4 is the meridional section of zonal current near the equator at 95°W for November 1982. Different

from Fig. 3's upper panel, Fig. 4's upper panel is a model derived variable, as opposed to a model variable that has been corrected by observations. The lower panel is the geostrophic calculation based on the observed temperature distribution. The calculation at and near the equator is based on Tsuchiya's (1955) method. The region of 95°W corresponds to NINO 3—that is, the eastern equatorial Pacific (150°–90°W)—and the Equatorial Undercurrent (EUC) is normally coincident with the shallow thermocline depth in this region. The 1982–83 El Niño has already commenced, and we see the surfacing of the EUC in both the DA and the geostrophic analysis. This comparison demonstrates not only the model's capability to simulate the quasigeostrophic nature of the temperature–velocity relationship but also that the assimilated model temperature field must have been similar to the observed one.

Figures 5a and 5b are latitude–depth diagrams of temperature and zonal current at 165°E, in the western Pacific, for January 1986. The observations were obtained by hydrographic casts and velocity profilers, mounted on a 20°S–10°N cruise, under a special TOGA program of the ORSTOM Centre in Nouméa, New Caledonia (Delcroix et al. 1987). Comparison between the DA and observations in Fig. 5a show remarkable similarity for all of the major features. Centered about the equator isotherm spreading associated with the EUC is observed. Below 200 m, the isotherms bend concave downward symmetrically about the equator, as required if the EUC is to be in geostrophic balance. The isotherms are convex upward between 140 and 200 m, but no evidence of equatorial upwelling is found above 140 m, which is contrary to the situation in the eastern (Fig. 15) and central (Fig. 13) Pacific. North of 4°N, the rising and steepening of the thermocline correspond to the North Equatorial Countercurrent (NECC) extending to 9°N. A pool of warm water with temperatures above 29°C is in the surface layer, within 17°S and 5°N, asymmetric about the equator; with the warmest water (>30°C) located between 10° and 3°S over a depth range of 60 m. In the section on zonal current (Fig. 5b), the latitudinal position and the depth of the EUC correspond well between the measurement ($U_{max}$ = 50 cm s$^{-1}$ at a depth of 200 m) and the DA ($U_{max}$ = 40 cm s$^{-1}$ at a depth of 220 m); the eastward flowing NECC (9°–4°N), also agrees, but the intensities are different ($U_{max}$ = 60 cm s$^{-1}$ vs 30 cm s$^{-1}$). Two branches of the westward flowing South Equatorial Current (SEC) (4°N–5°S and 11°–15°S) also correspond between the observation and the DA, though their intensities are different. The underestimation of the strength of the current vectors appears to be a deficiency of this DA. If there was sufficient confidence in the wind field, the vertical mixing scheme could be tuned to get the amplitude of the currents better. It appears that the addition of TOGA data contributes to the overall improvement of the analysis.
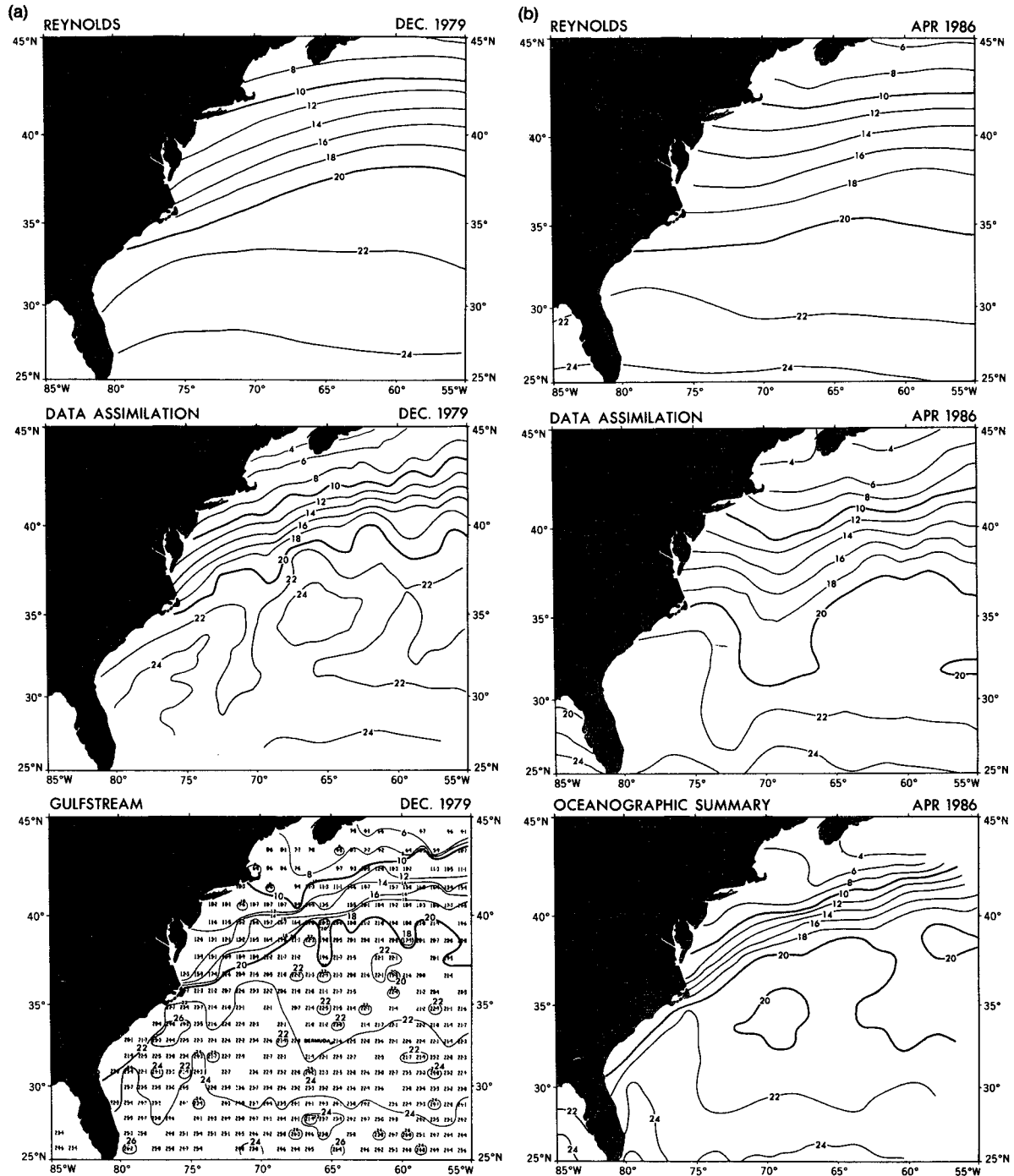
FIG. 7. (a) Sea surface temperature maps in the Atlantic Bight for December 1979. Isotherm contours are at an interval of 2°C: (top) Reynolds analysis; (middle) the data assimilation; (bottom) mean surface temperature plot for each 1° quadrangle where at least four observations were available (after *Gulfstream* 1980). (b) The same as (a) except for April 1986, and the temperature plot at bottom from *Oceanographic Monthly Summary* (1986).

## b. Maps of the Gulf Stream region

The simulation of the Gulf Stream or Kuroshio is a challenging task, because it is normally considered that an extremely high-resolution model is necessary to represent the oceanic mesoscale eddies. In this situation, it would be interesting to examine to what extent these mid-latitude small-scale features are reproduced by the 1° ×
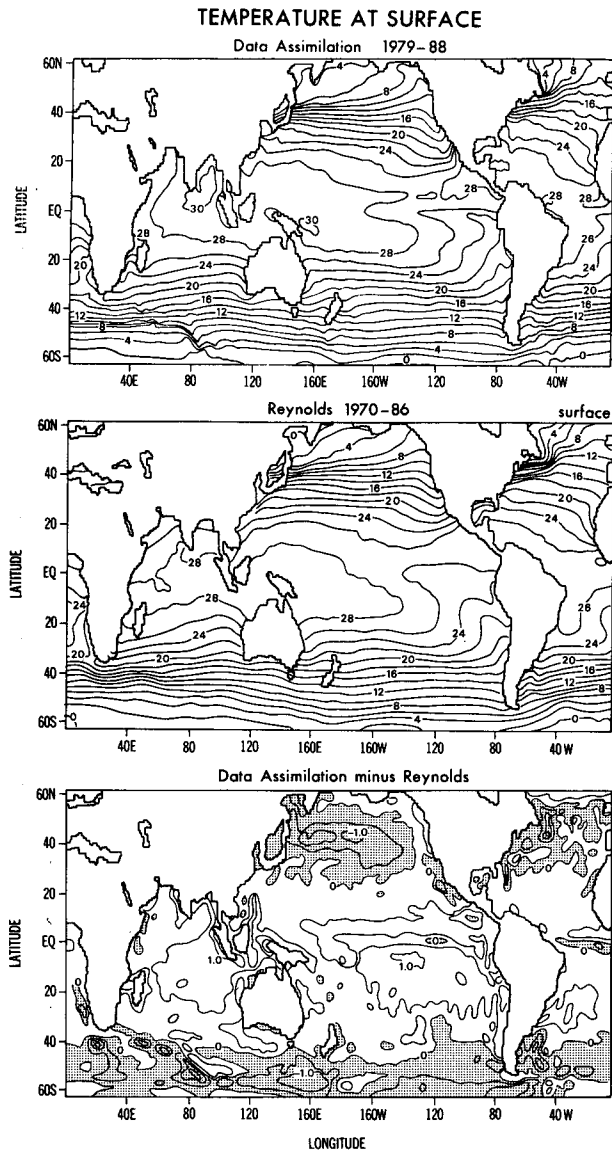
## TEMPERATURE AT SURFACE



FIG. 8. Maps of sea surface temperature, based on the decadal (1979–88) average of the data assimilation (top), the Reynolds (middle), and the difference (bottom). Contour interval is 2°C for the top and middle panels and 0.5°C for the bottom panel. The negative areas are stippled.

1° resolution model with the injection of observed data. It should be noted that, in the following figures, the frequency of reports and number of locations of observed data is essentially similar to those shown in Fig. 1.

Figure 6 shows the DA result for the SST and current vectors at the surface (3-m depth) over the western north Atlantic. It is most striking that the "separation of Gulf Stream" at Cape Hatteras has been successfully reproduced. This was not possible with just the "simulation," which uses the same forcing but no data insertion (not shown here). The ocean model tends to have a systematic bias toward the Gulf

Stream separating too far north. The XBT data together with the observed SST helped to produce an adequate "boundary current," so that the cyclonic recirculation develops to the north of the Gulf Stream and the southward flow along the coast between Cape Hatteras and Cape Cod. This implies that the coarse grid resolution is not a serious deficiency for the DA, as far as the location of the Gulf Stream separation issue and the general circulation. Nevertheless, more careful examination is needed to confirm whether the small-scale features of mesoscale eddies are really produced in the DA. An example of the Gulf Stream in the northwestern Atlantic Bight for December 1979 is shown in Fig. 7a. The middle panel of Fig. 7a is the SST from the DA, while the bottom panel is the direct plot of monthly average SSTs for each 1° quadrangle. This figure is taken from the monthly bulletin, *Gulfstream* (1980), and has been modified to fit the format of the other two panels. The position of the Gulf Stream in the DA (middle panel) compares well with the direct plots (bottom panel); the 10° and 20°C isotherms, which define the Gulf Stream axis, are similarly located. However, the undulations of the meander do not agree. The top panel, Reynolds' SST analysis based on a spatial resolution of 6°, shows very smooth contours and no small-scale structure, and yet interestingly, the maximum and minimum values agree with that in the bottom panel. Figure 7b is another example for a different time period—that is, April 1986. The direct plots of monthly average SST are taken from the monthly bulletin, *Oceanographic Monthly Summary* (1986). The two analyses produce markedly different Gulf Stream meanders. Upon examination into the dissimilarity between the two analyses, it was found that the COADS data, because it is averaged over 2° squares, did not contain enough resolution to resolve those coastal features. Hence, the DA would be biased toward the coarser COADS data. Another possible source of error could be that the statistics in the DA system—such as those contained in the first guess error covariance matrix and the observational error covariance matrix, which determine the spacial structure and amplitude of the temperature correction field—are not representative of this area. Changes to the statistics did have an influence on the patterns but did not bring the two analyses into agreement.

The overall features in the three types of SST maps, both in Figs. 7a and 7b, are similar to each other. Even though the eddies are so small that the 1° × 1° mesh cannot resolve them properly, this resolution clearly captured the large-scale circulation (e.g., the separation of the Gulf Stream) and thus the 1° × 1° grid is acceptable for the DA.

## 4. Decadal means

In this section we compare the 10-yr mean of the DA, which will be considered a climatology, with in-
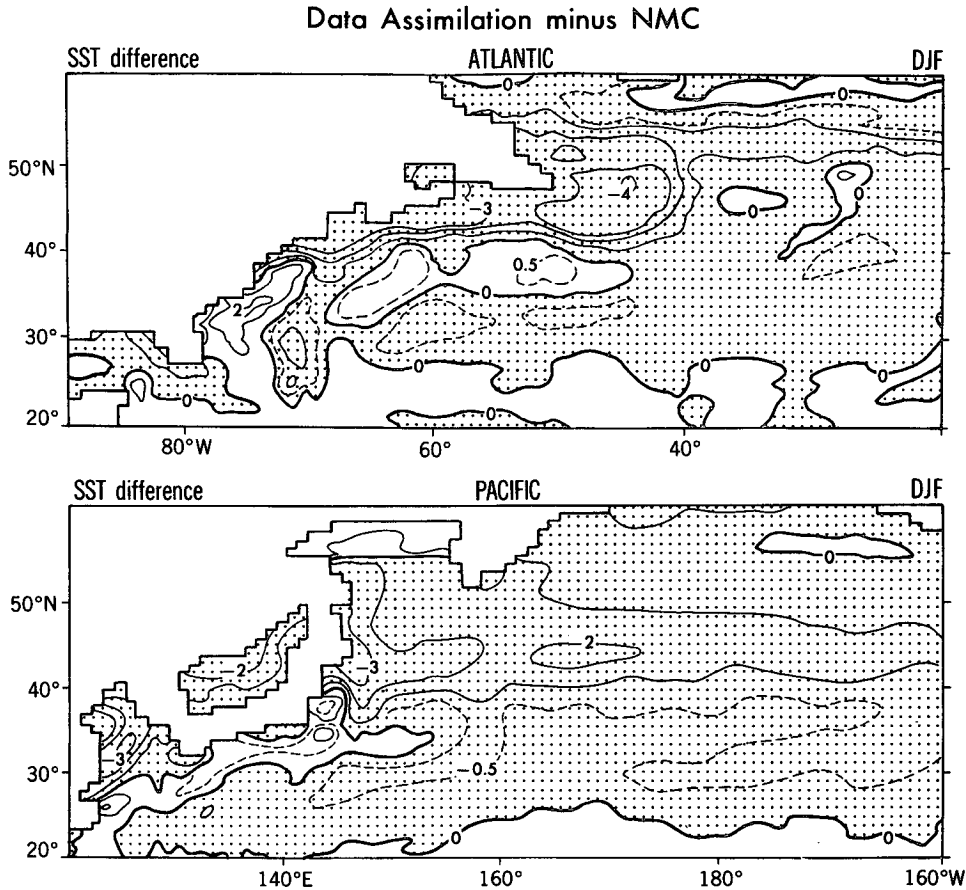
FIG. 9. Enlargements of the SST difference of 10-yr average (see Fig. 8)—i.e., the data assimilation minus Reynolds—over the northwestern Atlantic (upper) and the northern Pacific (lower), for December–February. Solid contour intervals are 1°C and the dashed contour intervals are 0.5°C. The negative areas are stippled.

dependent climate analysis. We define the mean and the deviation as below:

$$\text{mean} \quad \overline{(\;\;)} = \frac{\displaystyle\int_0^{10\ yr} (\;\;)dt}{\displaystyle\int_0^{10\ yr} dt} \qquad (4.1)$$

and

$$\text{deviation} \quad (\;\;)' = (\;\;) - \overline{(\;\;)}. \qquad (4.2)$$

### a. SST

Figure 8 is the annual mean SST, which is compared with that of NMC analysis, Reynolds (1988), Reynolds and Marsico (1993). The top panel is the 10-yr average from the DA, Eq. (4.1), the middle panel is Reynolds climatology from 1970 to 1986, and the bottom panel is the deviation, Eq. (4.2). The largest differences (>1°C) are found off Newfoundland, around Marvinas, over the Southern Ocean, and the extension of the

Kuroshio Current. In general, the large differences are predominantly negative, and they are located in the middle latitude, implying that the SSTs in the DA are lower than in Reynolds. Although not shown, the largest negative differences are associated with the winter hemisphere. This may imply a bias in the surface heat flux forcing. Overall the agreement is quite reasonable; however, in the regions where ocean dynamics play a dominant role, the differences are largest. To illustrate this point, we show in Fig. 9 SST differences from the 10-yr mean over the northwest Atlantic and over the northwest Pacific, respectively, for December–February. The map over the Atlantic (the top panel of Fig. 9) reveals again the characteristic differences of the Gulf Stream location and gradient between the DA and NMC analysis, as previously discussed in Figs. 7a and 7b. The differences are such that the northern part is dominantly negative and the southern part is positive, implying that the isotherms are located relatively southward in the DA. In other words, the isotherms in the DA are concentrated along the Gulf Stream, while those in the NMC are overly smoothed. This feature is
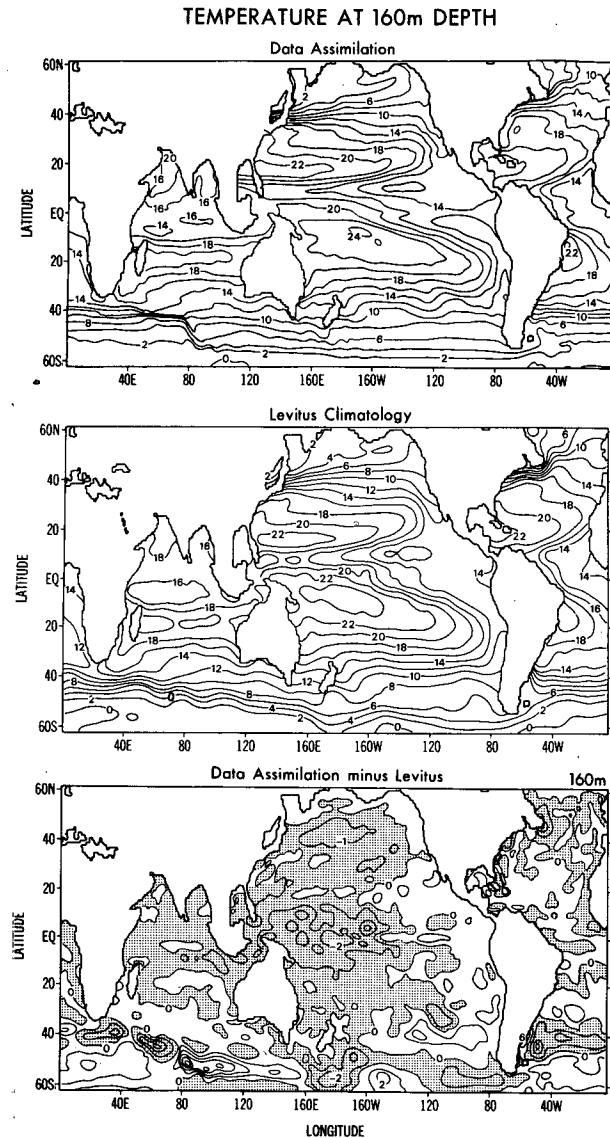
## TEMPERATURE AT 160m DEPTH



FIG. 10. Temperature at 160-m depth. The data assimilation (top), Levitus map (middle), and the difference—i.e., the data assimilation minus Levitus (bottom). Contour interval is 2°C in the top and middle panels, and it is 1°C in the bottom panel, where the negative areas are stippled.

stronger in December–February than in June–August (not shown here). The map over the Pacific (the bottom panel of Fig. 9b) shows similar differences; however, they are related to the Kuroshio current.

### b. Comparison with Levitus climatology

One interesting feature to consider is how well the DA system compares with established climatological datasets such as Levitus. This method, therefore, may be considered as a precursor toward producing climatological datasets that are dynamically constrained as

well as objectively analyzed. Toward this goal, a consistent forcing field, such as the CDAS product (Climate Diagnostic Analysis System, see Kalnay et al. 1993), would help to produce an oceanic analysis that includes interannual variability and climate trends. For this study, we have a fixed ocean DA system; however, the atmospheric DA from NMC was subject to many modifications during this time period; therefore, we lack consistent forcing. Nevertheless, we will compare the DA 10-yr mean as if it were a climatological dataset to the Levitus dataset.

Figure 10 shows the annual mean isotherms at 160-m depth in the DA and in Levitus (1982). The agreement is surprisingly good. Although here, as in Fig. 3, the DA is colder at depth in the high latitudes, indicating that winter convective mixing is deeper, and also in the western tropical Pacific, indicating that the thermocline is shallower. The discrepancies larger than 2°C exist near the date line along the equator, and also in the Southern Ocean, Newfoundland, and Marvinas. Figure 11 shows the seasonal cycle of the climatological thermocline depth in the equatorial Pacific (2°N–2°S). The time–longitude charts of the contours of 20°C depth are compared among the temperature nudging (first strip from left), the temperature–wind nudging (second strip), the DA (third strip), and Levitus data (fourth strip, that is, far right). The results of the DA and the nudging are the decadal averages, while the Levitus result is based on climatology. This figure reveals that the phase of the annual cycle, most pronounced in the east, agrees between the DA and Levitus, to a reasonable extent; the minimum depth is during September–October, and the maximum depth is during May–June. There is, however, a distinct difference west of the date line; the depth in the DA is shallower by about 10–20 m than that in Levitus, reflecting the temperature difference by 2°C in the bottom panel of Fig. 10. On the other hand, the annual cycle of the temperature nudging (first strip) shows a deeper thermocline depth from those of the other analysis, particularly in the western part of the basin. Perhaps the largest difference of the temperature nudging is the amplitude; the magnitude of the annual cycle in the temperature nudging is very large, whereas that of the temperature and wind is smaller.

One way to see how well the model simulates the seasonal cycle in the upper ocean is to examine mixed-layer depth (MLD). Figures 12a and 12b display the MLD in a time–longitude section along various latitude bands, for both Pacific and Atlantic basins. Here the DA is compared to the climatological MLD after Levitus. Overall, the agreement between the two analyses is good; however, the tropical bands do show significant differences.

Within the tropical band, (2.5°S–2.5°N), the characteristic east–west slope of the thermocline, deep in the central and western part of the basins as compared to the very shallow mixed layer in the east may be seen.
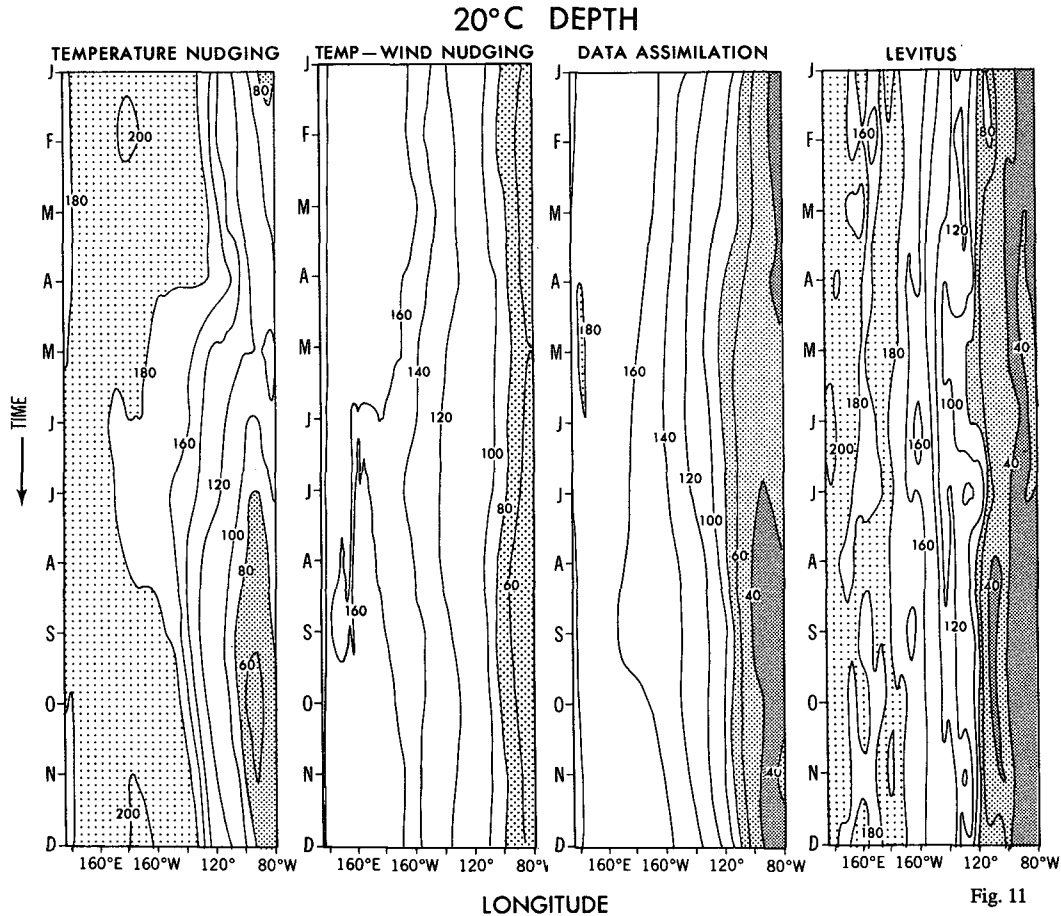
## 20°C DEPTH



FIG. 11. Annual cycle of the depth of the 20°C isotherm along the equator. From left to right, temperature nudging, temperature–wind nudging, data assimilation, and Levitus. Contour interval is 20 m.

This basic equilibrium state is simulated by the DA, also seen in the (2.5°–10°N) band, although it tends to be not as deep as the Levitus climatology. This is consistent with Fig. 10. The model tendency toward a shallower equatorial thermocline in the western Pacific is discussed in Rosati and Miyakoda (1988). The seasonal cycle is evident for the 10°–20°N and 20°–40°N bands. The DA seems to be quite reasonable, with the phase and amplitude of the maximum and minimum in the correct place. The MLD, within the 20°–40°N band for the western region during the winter does appear to be slightly deeper, perhaps due to excessive convective overturning.

### 5. Temporal variations in the tropical Pacific

From the standpoint of climate variability in the atmosphere–ocean coupled system, the influence of the tropical Pacific SST appears very profound. In particular, the phenomenon, called El Niño–Southern Oscillation (ENSO), has a large impact on the state of the global atmosphere and ocean for timescales from sea-

sonal to interannual (Ropelewski and Halpert 1987). For this reason, it is worthwhile to pay special attention to the results of the DA in this area. The DA system is not only important to study the interannual variability as a source for verification but also to produce oceanic initial conditions for coupled model forecasts.

### a. Time–depth charts

Figures 13 and 14 are the time–depth charts of temperature and u component at the central equatorial Pacific (159°W longitude), comparing the DA (middle panel) with the observations (bottom panel). The bottom panel is a direct plot of ship track measurements over a 16-month time span, which is based upon absolute current profilers, under the program of Pacific Equatorial Ocean Dynamics (Firing et al. 1983), and is modified for the purpose of comparison in this paper. Note that the top panel displays the results of the *simulation,* which uses the same model configuration, initial conditions, and forcing as the DA but there is no insertion of data.
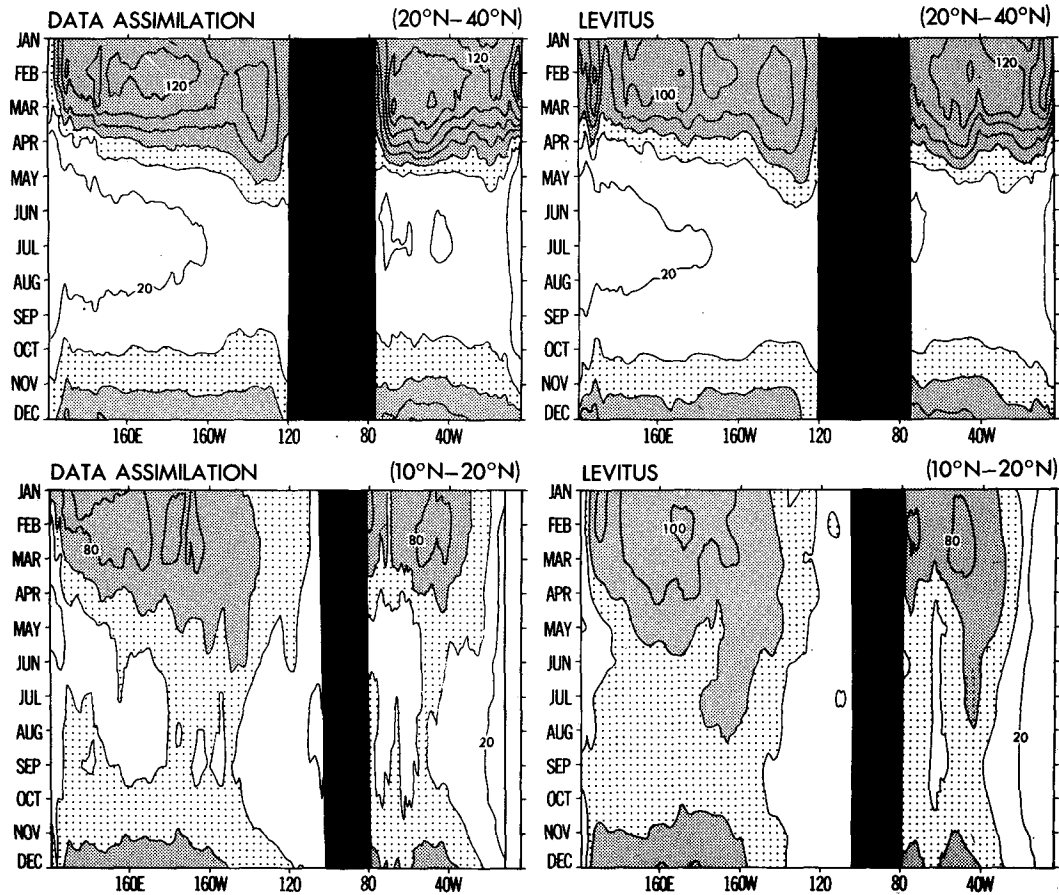
FIG. 12a. Time–longitude charts of mixed-layer depth by the data assimilation (left) and Levitus (right) for various latitudinal bands—i.e., (top) at middle latitude, 20°–40°N, and (bottom) at extratropics, 10°–20°N. Contour interval is 20 m.

One of the characteristic features in Fig. 13 is that the thermocline in the middle and lower panels is clearly visible at a depth of about 150 m; however, the simulation has a thermocline that is too diffuse. As one may note from the observations, there was an increase in the temperature of the surface layers but not a deepening of the thermocline. Then in December 1982 the thermocline rose, associated with the development of the El Niño. Both the simulation and the DA reproduce these changes, with the DA being more faithful to the data. The $u$ component in Fig. 14 represents a unique situation, associated with the El Niño. As Firing et al. mentioned, the EUC disappeared beginning in September 1982 continuing until early January 1983. The DA has some difficulty in reproducing the exact features of the zonal current (Fig. 14). The reason for the discrepancy is not clear; it could be due to some deficiency in the DA scheme or in the ocean GCM or the poor quality of the wind stress data.

Figures 15 and 16 are cross sections of temperature and zonal velocity along the equator at 95°W for 1982 and 1983. Once again the upper figures are the model

simulation, the middle figures are the data assimilation, and the lower figures are the observed values after Halpern (1987). The observations of Fig. 15 show the complex vertical structure of the evolution of heat content during the 1982/83 El Niño event at 95°W. We see the thermocline steadily deepening during 1982. In April and May 1983, we see a rise in SST rather than the continued deepening of the thermocline, and finally, in June 1983 the restoration to normal conditions [ for a more extensive discussion see Philander and Siegel (1984)]. Overall, the ability of the model to simulate these changes at the equator is demonstrated. Two serious flaws of the model simulation are the lack of a well-defined thermocline and the inability to return to normal conditions toward the end of 1983 (Rosati and Miyakoda 1988; Derber and Rosati 1989). Although these discrepancies may be related to errors in the wind field, we see that the DA does maintain a tight thermocline gradient and does recover from the El Niño after July 1983.

In Fig. 16 the observations show a deceleration of the EUC during 1982, the appearance of an eastward
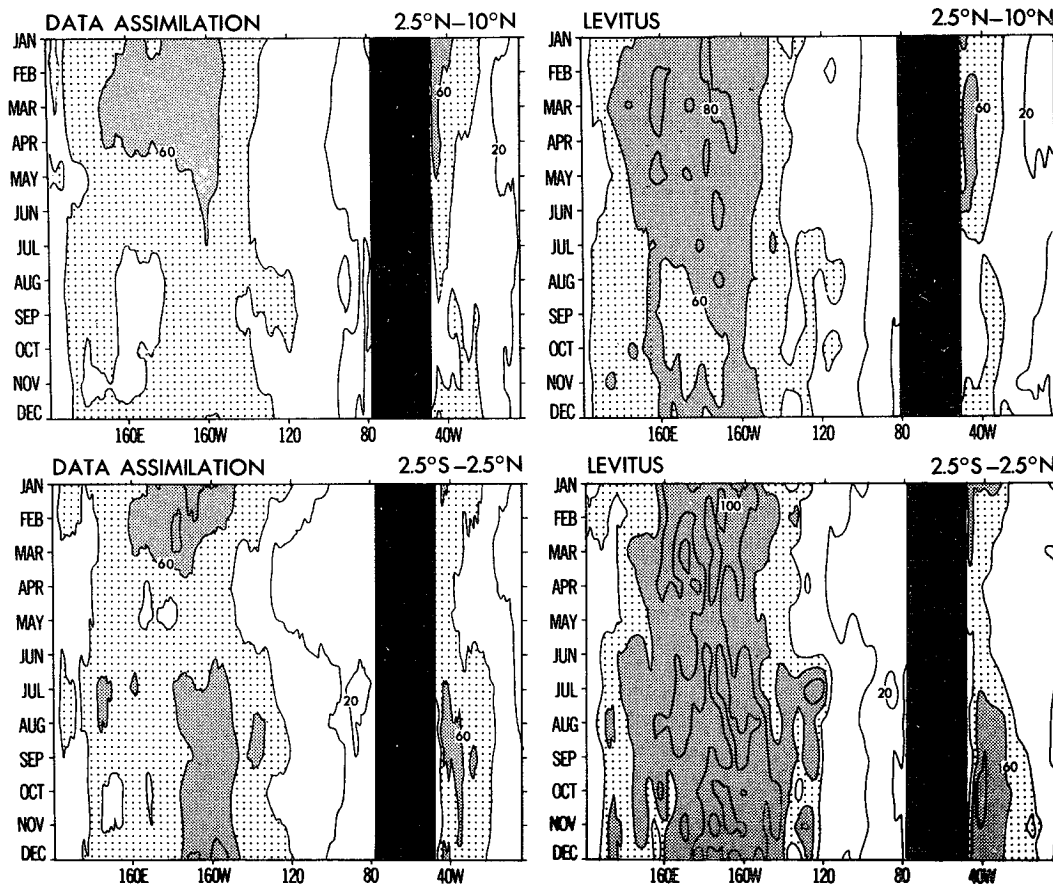
FIG. 12b. Same as Fig. 12a except for different latitudinal bands—i.e.,
(top) at 2.5°–10°N and (bottom) at the equator 2.5°S–2.5°N.

jet during April–June 1983, and finally, normal conditions. Once again the model simulates the gross feature. However, the major shortcomings are a considerable underestimation of the EUC speed and a poor simulation of the phase and return to normal. The data assimilation did show good agreement with observations for the temperature field; however, the zonal current sustains a strong easterly jet and does not show a timely return to normal conditions. Perhaps for the same reasons as mentioned for Fig. 14.

Figures 13–16 demonstrate the ability of the DA to simulate the changes in the vertical structure of the flow at locations with considerable differences in the variability. The extent to which errors in the surface boundary conditions, especially in the wind field, caused the discrepancies between the measurements and the model and to a lesser extent the DA are not completely known and will be assessed as the atmospheric surface analyses improve. For example, the EUC is driven by the eastward pressure force, which is maintained by the westward trades. Differences between strength of the EUC in the DA and the observations may well be due to the inconsistency between the wind stress and the

east–west slope of the density field inferred from the data.

## b. Hovmöller diagrams

Hovmöller diagrams in this paper are time–longitude or time–latitude plots of any variable. Figure 17 is the equatorial Pacific time–longitude diagram for the SST anomalies from 1981 to 1988. The left side is the result of the DA and the right side is the CAC (Climate Analysis Center, NMC) analysis (Kousky and Leetmaa 1989). The latter is based on the Reynolds SST analysis. The agreement between the two analyses—that is, the left and the right—is reasonable. Two El Niño (warm phase)—that is, 1982/83 and 1986/87—and two La Niña (cold phase)—that is, 1984/85 and 1988—events are clearly identified in the 140°–80°W sector. The largest differences are found in the western Pacific, and overall the maximum or the minima are more intense in the DA than in the Reynolds.

The seasonal variation of the depth of the 20°C isotherm along the equator was already shown in Fig. 11. The 20° isotherm runs in the middle of thermocline
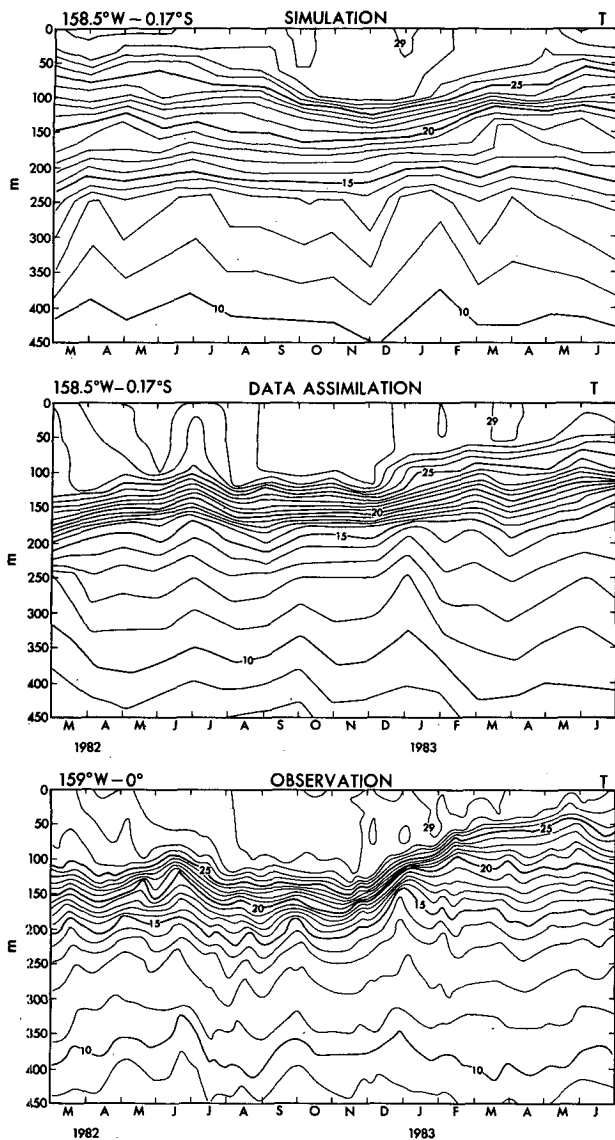
FIG. 13. Time–depth diagrams of temperature at the central equatorial Pacific—that is, 0°–0.17°S, 158°–159°W. Simulation (top), data assimilation (middle), and observation (bottom). Contour interval is 1°C.

along the equatorial belt throughout the Pacific, Atlantic, and Indian Oceans. Therefore, it has been customary to use the depth of 20°C isotherm as a measure of the available heat content in the upper ocean. In the NMC analysis, this depth has been monitored operationally as an index of ENSO (see Leetmaa and Ji 1989). Figure 18 is the time series from 1985 to 1988 of the depth of the 20°C isotherm based on the DA and also the DA as calculated by Leetmaa and Ji (1989). The two diagrams agree with each other reasonably well, and yet, one wonders why they are different, considering that both analyses are based on the same model

and also the same DA scheme. The explanation may be attributed to a number of factors: (a) the forcing data, (b) the ocean model configuration, (c) quality control and quantity of data, and (d) statistics used in DA.

Next we examine the relation between the heat content and 20°C isotherm. The heat content defined in this paper is the part contained in the upper ocean from the surface to the 248-m depth (the 11th level), and computed by

$$\text{heat content} = \int_{-248\text{ m}}^{0} \rho C_p T dz, \qquad (5.1)$$

where $\rho = 1.02$ g cm$^{-3}$ and $c_p = 4.187$ J (g K)$^{-1}$. Figure 19 shows Hovmöller diagrams of heat content,



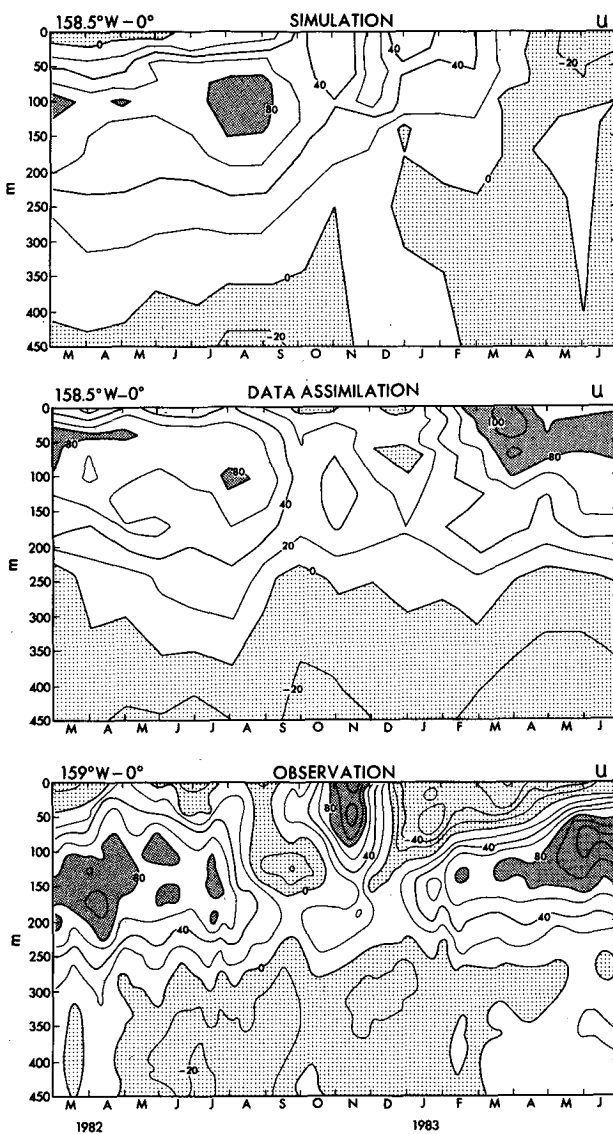FIG. 14. Same as Fig. 13 but for the zonal component of current, $u$. Contour interval is 20 cm s$^{-1}$. The areas of $u \geqslant 80$ cm s$^{-1}$ are shaded dark, and the areas of $u < 0$ are stippled.
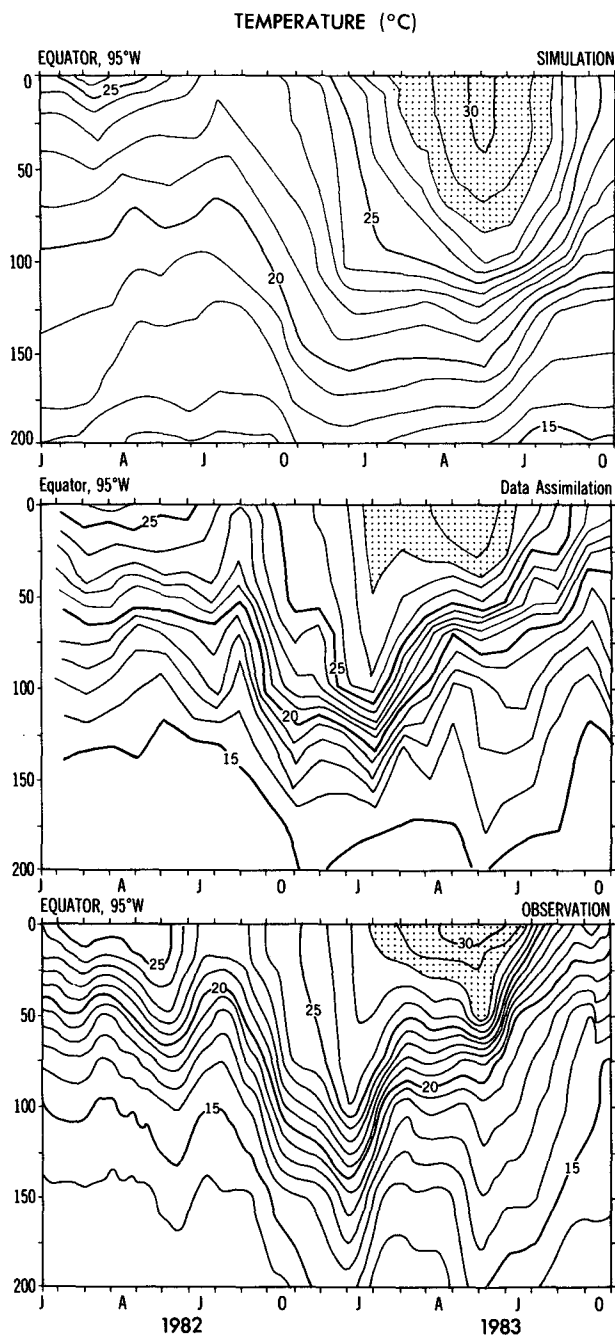
## TEMPERATURE (°C)



FIG. 15. Same as Fig. 13 except the location, the eastern equatorial Pacific—i.e., 0°–0.17°S, 95°W. The areas of greater than 28°C are stippled.

alies of these quantities also resemble each other very well (not shown here). This demonstrates that the depth of the 20°C isotherm is a good substitute for the variability of heat content, within the Tropics. The two nudging cases, the left and the middle panels in Fig. 19, do not show good agreement. The temperature
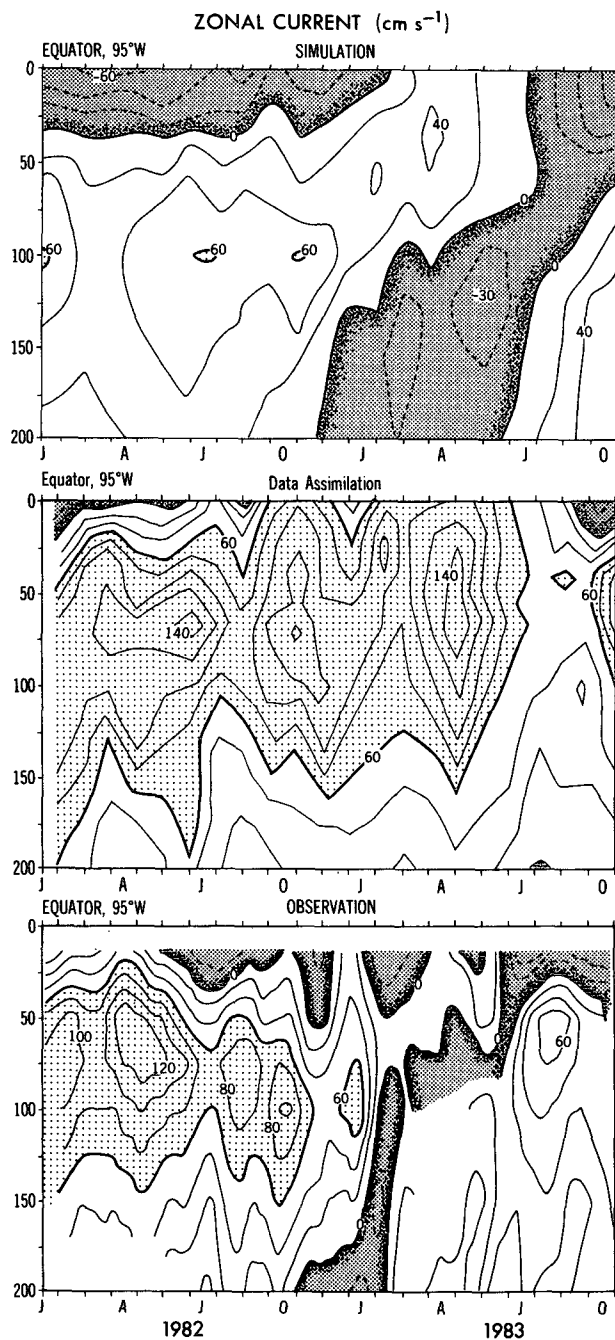
## ZONAL CURRENT (cm s⁻¹)



FIG. 16. Same as Fig. 14 except the location—i.e., 95°W (see Fig. 15). The areas of less than 0 cm s⁻¹ are shaded, and the areas of at least 60 cm s⁻¹ are stippled.

along the equator, for temperature nudging at the left, temperature-wind nudging in the middle and DA at the right. First it should be pointed out that the interannual variability, due to the rise and fall of the thermocline, has a similar signature in both the DA heat content as seen in Fig. 19 (right side) and the DA depth of the 20°C isotherm as seen in Fig. 18 (left side). The anom-
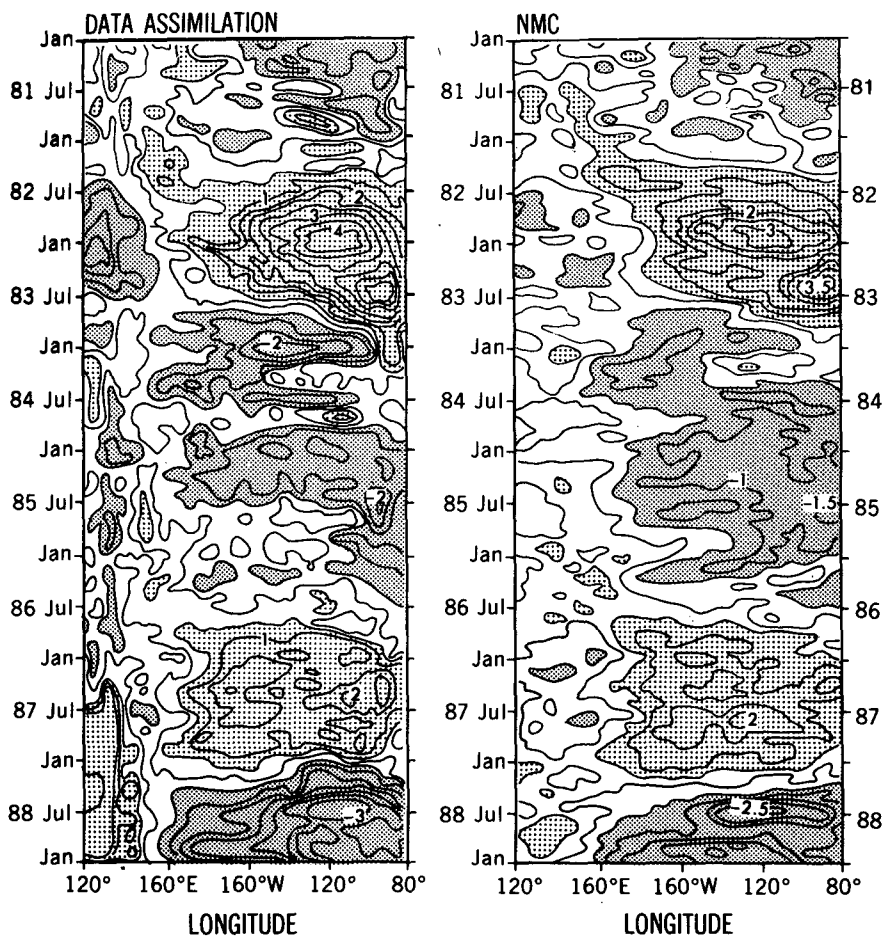
## SST



FIG. 17. Longitude–time diagrams of SST along the equator. The data assimilation (left),
and the NMC analysis (right). Contour interval is 1°C.

nudging case shows a pronounced annual cycle in the eastern part of the basin. Although this is a feature of the SST, observed annual variations in thermocline depth are weak; therefore, the annual cycle in heat content for this case is unrealistic. In the western part of the basin, the temperature nudging case contains much more heat than the other two cases. What this reveals is the sensitivity of the subsurface thermal field to the wind field. In the temperature nudging case the winds that drove the ocean model were generated from the atmospheric model. Examination of the model winds showed stronger than observed westerlies in the western equatorial Pacific during December–February. This resulted in convergence at the equator and caused downwelling, which influxed a large amount of heat into the ocean. This was possible since the model surface temperature was being forced to observed SSTs; therefore, there was a positive heat flux into the ocean. In the coupled system, this wind bias increases evap-

oration and reduces the heat flux into the ocean resulting in SSTs that are too cold. When the observed wind field (NMC analysis) is used the systematic westerly bias is removed and a more reasonable heat content is simulated, as shown in the temperature-wind nudging and DA cases. It was also found that the atmospheric model had a bias toward trade winds that were too strong. Without the SST flux adjustment this would have resulted in increased upwelling and SSTs that would be too cold in the central and eastern Pacific. However, with the flux adjustment, enormous amounts of heat had to be fluxed into the ocean model, to maintain the observed annual cycle of SST, due to the systematic error in the model wind field. This resulted in the pronounced annual cycle in the heat content. Looking at the heat content over the central Pacific, a much tighter gradient may be observed in the DA as opposed to the other two cases. Once again this shows that the ocean model produces too diffuse a thermocline, and

## 20°C DEPTHS

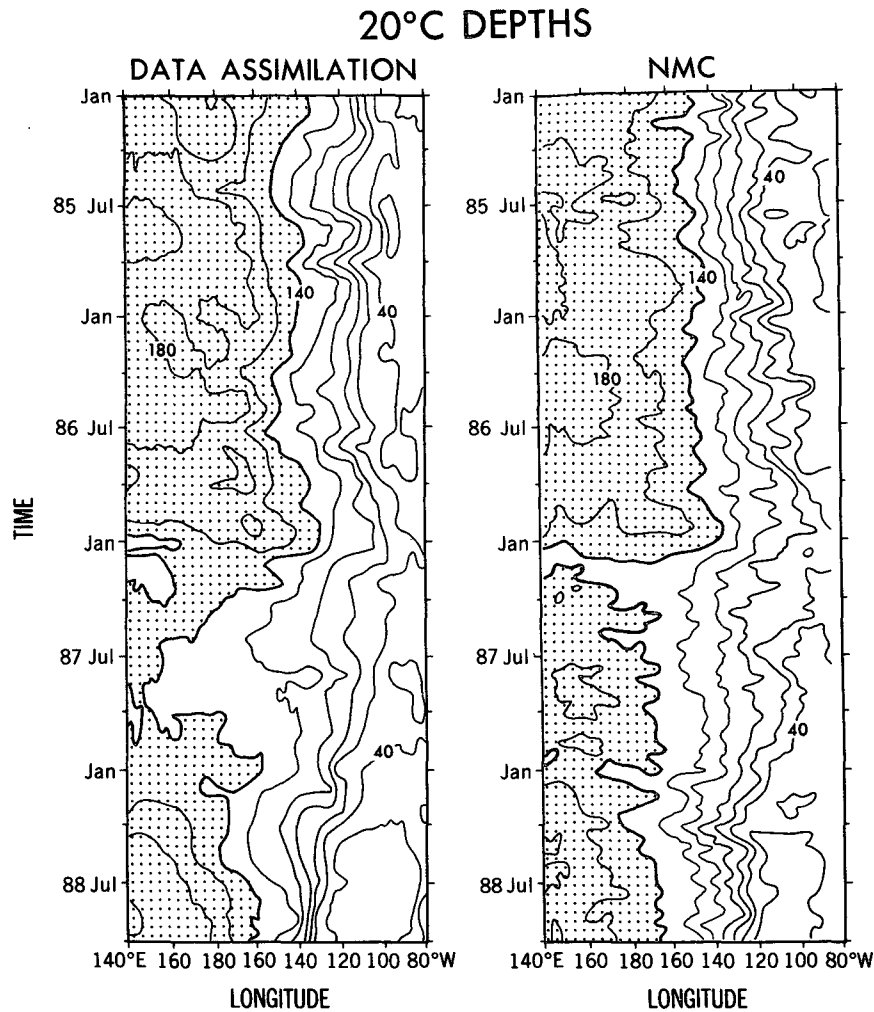### DATA ASSIMILATION                    NMC



FIG. 18. Longitude–time charts of the 20°C depth along the equatorial Pacific Ocean, based on the data assimilation (left) and on the NMC (right). Contour interval is 20 m. The thick contours are for 140 m.

that this bias may be alleviated by the addition of sub-surface data in the DA.

### c. ENSO signature

Figure 20 shows time–longitude diagrams of the heat content anomalies along the equator, in the Pacific, from 1981 to 1988. As in the previous figure, the right panel is the DA; the middle is the temperature–wind nudging; and the left is the temperature nudging. Where the total heat content showed distinct differences between the three assimilations, the anomalies, about their individual means, show that the interannual fluctuations of the thermocline are similar.

As in Fig. 17, the most pronounced feature in Fig. 20 is the two distinct episodes of El Niño and La Niña, and that these positive and negative anomalies of heat content propagate from west to east. With regard to this propagating signature, it may be interesting to compare this diagram (the right panel) with the diagram of SST anomalies (the left panel of Fig. 17). The two El Niño signatures are fairly evident; however, the 1986/87 event is more distinct in the SST anomalies than in the heat content anomalies, and for the whole period, the eastward propagation is dominant in the heat content, as opposed to some element of westward propagation in the SST. This coherence between SST anomalies and heat content anomalies appears to be essential to ENSO predictability. It would seem of paramount importance that the assimilation scheme, used to produce initial conditions for ENSO forecasting, must contain an accurate representation of the phase and amplitude of these propagating heat content anomalies.

Figures 21 and 22 are time–latitude diagrams of the heat content anomalies that show the thermal processes in the meridional direction. Figure 21 is for the western
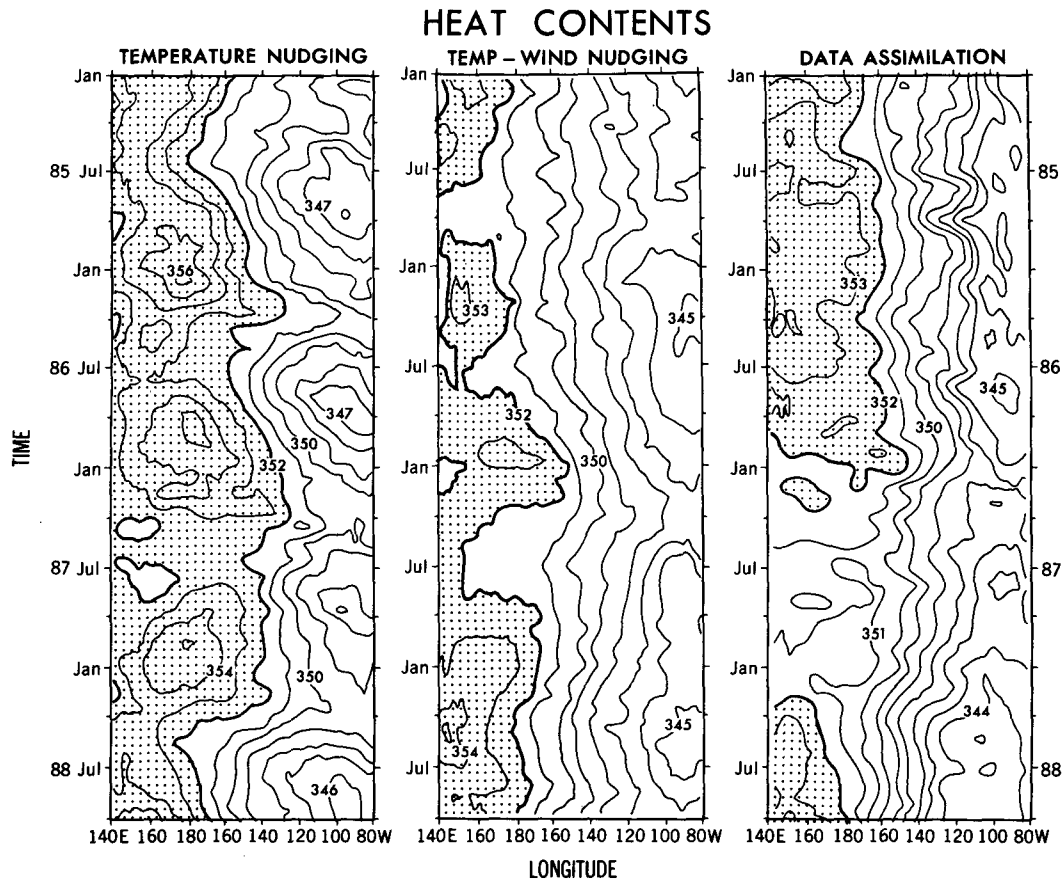
# HEAT CONTENTS



FIG. 19. Longitude–time charts of the heat content along the equator in the Pacific Ocean, based on the temperature nudging (left), the temperature–wind nudging (middle), and on the data assimilation (right). Contour interval is $10^9$ J m$^{-1}$. The thick contours are for $352 \times 10^9$ J m$^{-1}$.

Pacific averaged between 139° and 172°E, and Fig. 22 is for the eastern Pacific averaged between 141° and 81°W. The evolution of thermal structure within the equatorial Pacific basin (20°N–20°S) and its significance in the context of ENSO cycle has been discussed extensively by, for example, White et al. (1985), Schopf and Suarez (1988), and Wakata and Sarachik (1991). In the western Pacific DA (the right panel of Fig. 21), the positive anomalies emerge from July 1981 to July 1982, and also from July 1985 to July 1986, while the negative anomalies are found between these two episodes. These positive anomalies are spread over a 20°N–20°S belt with the maxima off the equator. On the other hand, in the eastern pacific (the right panel of Fig. 22), the positive anomalies are identified with the maxima at the equator from July 1982 to July 1983, and also from January 1986 to July 1987. These features appear to fit reasonably well the scenarios of ENSO cycle, in which the heat recycling processes are due to eastward-propagating Kelvin waves and westward-propagating Rossby waves. Intercomparison between the assimilation systems shows that there is fair

agreement in phase but the amplitude does not agree well. The agreement in phase indicates that the anomalous rise and fall of the thermocline is captured. The differences between the two nudging schemes shows the effect of the winds and the largest differences in amplitude appear to be in the eastern part of the basin (Fig. 22) where the thermocline is shallow. The fact that the nudging cases are showing such little variability is indicative of the lack of variance in the wind field. In the temperature nudging case it may be indicating that the coupled model wind field is not responding well to the SST anomalies.

## 6. Summary and conclusions

A global oceanic data assimilation system has been developed. This data assimilation system was created primarily for the initialization of coupled ocean–atmosphere models for use in producing seasonal forecasts. We examine the fields produced by the assimilation procedure, over the 10-yr period that was run, both for their temporal variability and as a climatological dataset.
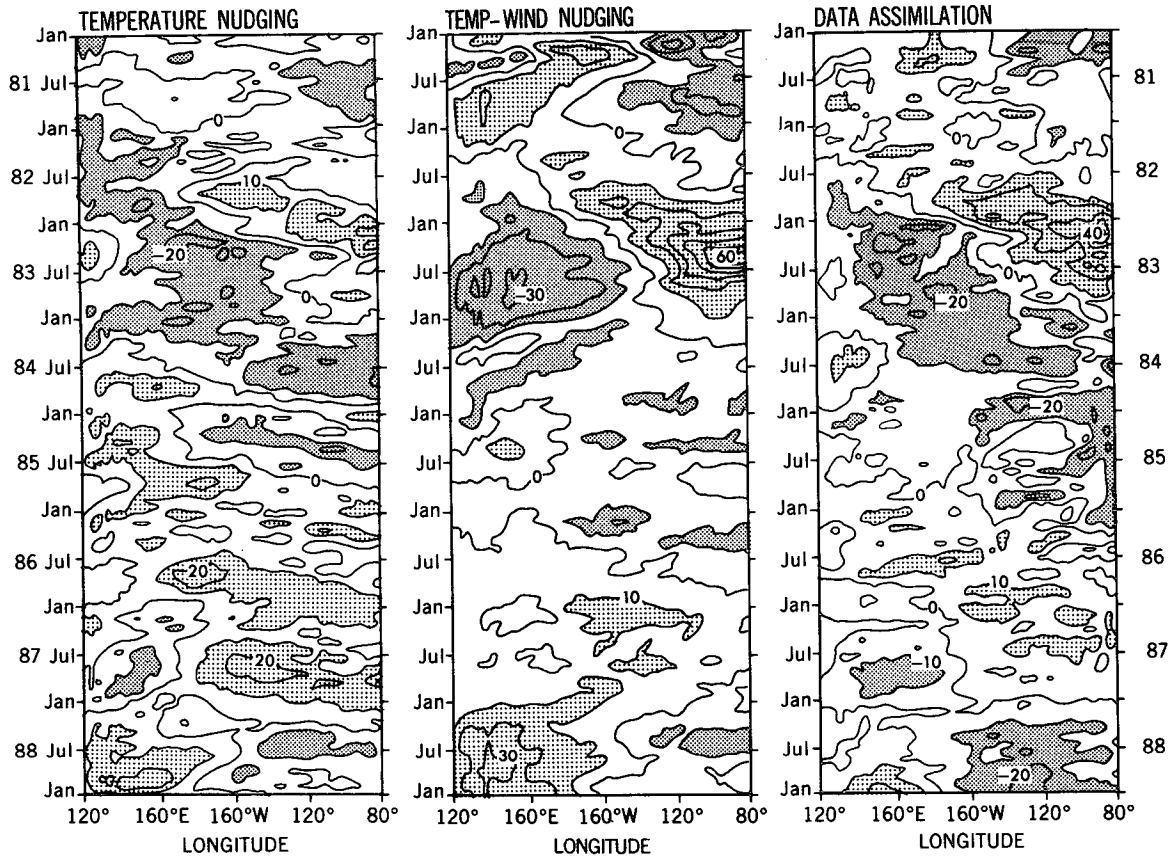
## HEAT CONTENT ANOMALIES 4°N–5°S



FIG. 20. Longitude–time diagrams of ocean heat content anomalies along the equator from the temperature nudging (left), the temperature–wind nudging (middle), and the data assimilation (right). Contour interval is $10^9$ J m$^{-1}$. Regions larger than $10 \times 10^9$ J m$^{-1}$ and less than $-10 \times 10^9$ J m$^{-1}$ are stippled differently.

The ocean data used in the DA system consisted only of conventional temperature observations. For surface observations, 2° × 2° COADS data (Woodruff et al. 1987) were used. Vertical temperature profiles were incorporated from NODC and the U.S. Navy's MOODS dataset. While the coverage of the sea surface temperature data was quite good during this period, the vertical temperature profile data contained large gaps, particularly, in the equatorial region and in the Southern Hemisphere.

The assimilation procedure was developed using a modified version of a global high-resolution numerical model developed by Rosati and Miyakoda. This model is based on the primitive equations with the atmospheric forcing provided from the 12-h atmospheric analysis of NMC. The data were inserted into the model using a continuous insertion technique. A temperature correction field was created and inserted into the model solution. Instead of creating a correction field every time step, it was found that quite a computational savings could be realized, without compromising quality, by calculating a new correction for three consecutive

time steps and then applying the last correction for nine time steps. The temperature correction was created by applying a statistical objective analysis routine to the differences between the model solution and the data in a 30-day window around the analysis time step.

The results from the assimilation system applied over the decade from 1979 to 1988 are encouraging. The SST fields compare well to the operational analyses in terms of large-scale features. For smaller scales, the analysis captures some features not contained in the operational analyses, but it probably contains too much noise. At subsurface levels, the model solution is made much more realistic by the inclusion of data. The decadal means compared well in the upper ocean with the established climatologies of NMC SST analysis and Levitus. Their agreement is of particular interest since the basis of the DA is a dynamical model, whereas the other two use objective analysis. This bodes well for ocean DA as a source for future climatologies, since one could expect that as the numerical model improves so will the analysis. Another advantage would be that the DA would also contain mean information about the
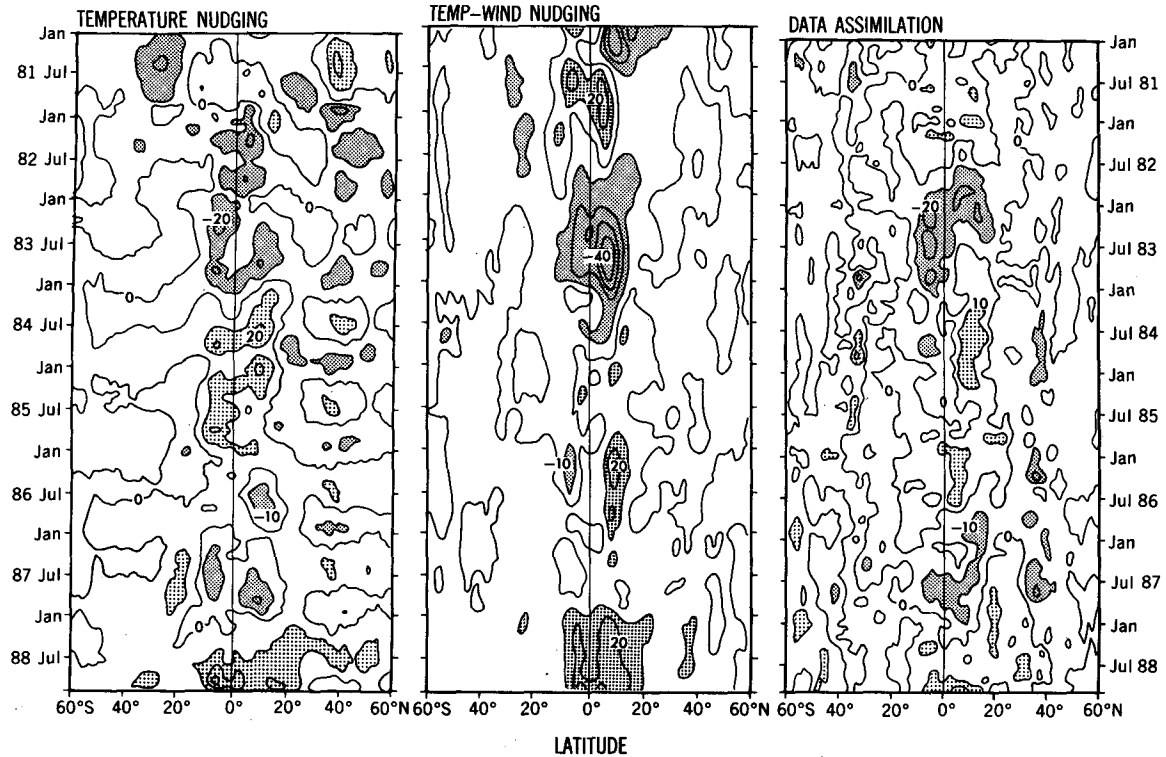
HEAT CONTENT ANOMALIES 139°–172°E



FIG. 21. The same as Fig. 20 except the latitude–time diagram for the western Pacific.

general circulation. The interannual variability was compared to a variety of analyses for the tropical Pacific and it was found that the DA captured the main features of the thermal structure including the ENSO signature. Although the velocity structure did not agree as well with observations. The ability of the DA to realistically simulate the variability on seasonal to interannual timescales has led to using it to provide initial conditions and verification fields for the experimental seasonal forecasts of the coupled model.

As a first step toward producing a self-consistent data assimilation system for coupled models, whereby the atmosphere and ocean model are in balance with one another, two other schemes were investigated. These procedures were based on using the coupled model using Newtonian nudging of SST and then SST and surface wind forcing. The nudging systems produced very different heat contents as compared to the DA system. It would appear, that at least for the present model, the wind field is not enough to define the subsurface thermal structure correctly. Although the SST–wind nudging was more realistic than the SST only. The only difference between the two runs was the wind forcing, thus indicating, not only, the sensitivity to atmospheric forcing, but also, that the coupled model winds are not very good.

The assimilation procedure may be improved by expanding the database and by improving the quality control. Since the period of this study, only a fraction of the TOGA TAO data was available. The assimilation should be substantially improved, in the tropical Pacific, with the addition of this database. Also, the database may be expanded by using other observation types, such as satellite-derived SSTs, altimetry data, and current measurements.

Changes to the assimilation procedure itself can also enhance the results. The statistics currently in use in the statistical objective analysis scheme are somewhat ad hoc. The first-guess error statistics are obviously deficient since they vary only in the meridional direction. The ocean dynamics are very different in regions with strongly sloping bottom topography or along the equator. The model's error characteristics are quite different in these regions because of this and should be accounted for in the first-guess error covariances. With improved knowledge of the model's and the data's error characteristics many of the errors in the present system may be reduced.

Any improvements to the numerical model solution feeds back to improve the analysis produced by the assimilation system. These improvements may be made directly to the model dynamics or physics, or may enter
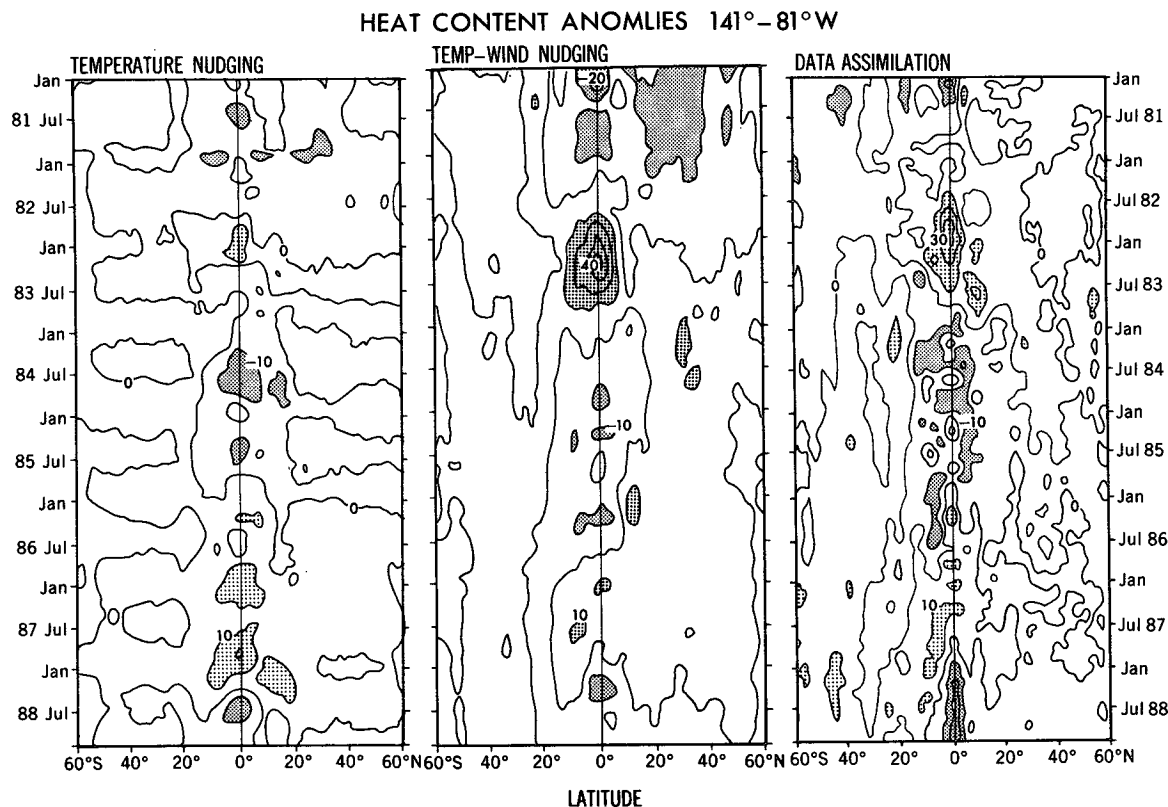
HEAT CONTENT ANOMLIES 141°–81°W



FIG. 22. The same as Fig. 20 except the latitude–time diagram for the eastern Pacific.

through atmospheric forcing. At this point in time, the effects of inaccurate atmospheric forcing on the assimilation are not completely known. Given the complexity of the whole system, that is, the data and its associated errors and distribution; the ocean model with unknown impacts from resolution and physics parameterizations; the assimilation procedure with the difficulty in specifying error statistics; and the extent to which errors in the atmospheric forcing cause problems, it is extremely difficult ascertain where things go wrong and why. It seems obvious, however, that one can still produce useful and reasonable solutions from the present DA system. The incorporation of all potential enhancements can only improve the results.

## REFERENCES

Bauer, R. A., 1985: Functional description Master Oceanographic Observation Data Set (MOODS). FNOC, 477 pp. [Available from Fleet Numerical Oceanographic Center, Monterey, CA 93940.]

Carton, J. A., and E. C. Hackert, 1990: Data assimilation applied to the temperature and circulation in the tropical Atlantic, 1983–84. *J. Phys. Oceanogr.,* **20,** 1150–1165.

Delcroix, T., G. Eldin, and C. Hénin, 1987: Upper ocean water masses and transports in the western tropical Pacific (165°E). *J. Phys. Oceanogr.,* **17,** 2248–2262.

Derber, J., and A. Rosati, 1989: A global oceanic data assimilation system. *J. Phys. Oceanogr.,* **19,** 1333–1347.

Firing, E., R. Lukas, J. Sades, and K. Wyrtki, 1983: Equatorial undercurrent disappears during 1982–1983 El Niño. *Science,* **222,** 1121–1123.

Gandin, L. S., 1966: *Objective Analysis of Meteorological Fields* (translation). Israeli Program for Scientific Translations, 242 pp.

Ghil, M., and P. Malanotte-Rizzoli, 1991: Data assimilation in meteorology and oceanography. *Advances in Geophysics,* Vol. 33, Academic Press, 141–266.

Gordon, C. T., and W. F. Stern, 1982: A description of the GFDL global spectral model. *Mon. Wea. Rev.,* **110,** 625–644.

Gulfstream, 1980: Monthly summary for December 1979. *Gulfstream,* **5**(12), 7 pp.

Halpern, D., 1987: Observations of annual and El Niño thermal and flow variations at 0°, 110°W and 0°, 95°W during 1980–1985. *J. Geophys. Res.,* **92**(C8), 8197–8212.

Hellerman, S., and M. Rosenstein, 1983: Normal monthly windstress over the World Ocean with error estimates. *J. Phys. Oceanogr.,* **13,** 1093–1104.

Kalnay and Coauthors, 1993: The NMC/NCAR CDAS/Reanalysis Project. NMC Office Note 401.

Kessler, W. S., 1989: Observations of long Rossby Waves in the northern tropical Pacific. *Proc. Western Pacific International Meeting and Workshop on TOGA COARE,* Nouméa, New Caledonia, ORSTROM, 185–203.

Kousky, V. E., and A. Leetmaa, 1989: The 1986–87 Pacific warm episode: Evolution of oceanic and atmospheric anomaly fields. *J. Climate,* **2,** 254–267.

Leetmaa, A., and M. Ji, 1989: Operational hindcasting of the tropical Pacific. *Dyn. Atmos. Ocean,* **13,** 465–490.

Levitus, S., 1982: Climatological Atlas of the World Ocean. NOAA Prof. Paper No. 13, U.S. Govt. Printing Office, 183 pp.

Lorenc, A., 1986: Analysis methods for numerical weather prediction. *Quart. J. Roy. Meteor. Soc.,* **112,** 1177–1194.

Miyakoda, K., J. Sirutis, A. Rosati, and R. Gudgel, 1989: Some activities at GFDL relevant to COARE. *Proc. Workshop on Japanese-Coupled Ocean Atmosphere Response Experiments,* 93–104.

Oceanographic Monthly Summary, 1986: *Oceanogr. Mon. Sum.,* **6**(4), 24 pp.

Philander, S. G. H., and A. D. Seigel, 1984: Simulation of El Niño of 1982–1983. *Coupled Ocean–Atmosphere Models,* J. G. J. Nihoul, Ed., Elsevier Oceanography Series, No. 40, 517–541.

Reynolds, R. W., 1982: A monthly averaged climatology of sea surface temperature. NOAA Tech. Rep. NWS 31, Washington, DC, 33 pp.

——, 1988: A real time global sea surface temperature analysis. *J. Climate,* **1,** 75–86.

——, and D. C. Marsico, 1993: An improved real-time global sea surface temperature analysis. *J. Climate,* **6,** 114–119.

——, C. K. Folland, and D. E. Parker, 1989: Biases in satellite derived sea-surface temperatures. *Nature,* **341,** 728–731.

Ropelewski, C., and M. Halpert, 1987: Global and regional scale precipitation patterns associated with the El Niño/Southern Oscillation. *Mon. Wea. Rev.,* **114,** 2352–2362.

Rosati, A., and K. Miyakoda, 1988: A general circulation model for upper ocean circulation. *J. Phys. Oceanogr.,* **18,** 1601–1626.

Sasaki, Y., 1958: An objective analysis based on the variational method. *J. Meteor. Soc. Japan,* **36,** 77–88.

Sausen, R., K. Barthels, and K. Hasselmann, 1988: Coupled ocean-atmospheric models with flux correction. *Climate Dyn.,* **2,** 154–163.

Schopf, P. S., and M. S. Suarez, 1988: Vacillations in a coupled ocean–atmosphere model. *J. Atmos. Sci.,* **45,** 549–566.

Tsuchiya, M., 1955: On a simple method for estimating the current velocity at the equator. *J. Oceanogr. Soc. Japan,* **11,** 1–4.

Wakata, Y., and E. S. Sarachik, 1991: On the role of the equatorial ocean modes in the ENSO cycle. *J. Phys. Oceanogr.,* **21,** 434–443.

White, W. B., G. A. Meyers, J. R. Donguy, and S. E. Pazan, 1985: Short-term climatic variability in the thermal structure of the Pacific Ocean during 1979–1982. *J. Phys. Oceanogr.,* **15,** 917–935.

Woodruff, S. D., R. J. Slutz, R. L. Jenne, and P. M. Steuer, 1987: A comprehensive ocean–atmosphere data set. *Bull. Amer. Meteor. Soc.,* **68,** 1239–1250.